University of Alberta

A spectroscopic approach for inferring charcoal concentrations and fire history from lacustrine sediments

by

Emma Virginia Jones

A thesis submitted to the Faculty of Graduate Studies and Research
in partial fulfillment of the requirements for the degree of

Master of Science

Earth and Atmospheric Sciences

Fall, 2013
Edmonton, Alberta

ABSTRACT

Current wildfire activity highlights the precarious ecological state of forests owing to the combined effects of climate change and management practices. Because the analysis of long-term fire frequency from sedimentary archives is critical to understanding fire dynamics, there is a continuous need to refine methodologies used to reconstruct fire frequency and intensity. Visible-near infrared (VNIR) spectroscopy offers a rapid and non-destructive method for remotely sensing charcoal concentrations from lacustrine sediment cores. In this study, a predictive model for quantifying charcoal concentrations from lake sediment absorbance was developed and subsequently applied to an 8000 year sediment record from Grand Teton National Park (Wyoming, USA). This record provides a detailed continuous fire history that captures regional fire trends obtained by optically counted charcoal from nearby lakes. The novel spectroscopic method for charcoal quantification reduces laboratory processing time tremendously and avoids various biases associated with conventional optical microscopic charcoal enumeration techniques.

ACKNOWLEDGEMENTS

This manuscript would not have been possible without the concerted efforts of a few key mentors and loved ones. Foremost, I would like to thank Alex Wolfe for his inspiration and the opportunity to learn in this academic environment. Without his constant encouragement, guidance, and faith in both myself and the project, I would most certainly have been lost. Assistance from Neal Mitchelutti, Trevor Porter, and Will Hobbs was integral to my research experience, supporting all my laboratory and statistical endeavors. I'd also like to thank Sarah Spaulding for her efforts in sample procurement and in the field and David Roberts for answering my never-ending list of R questions. Benoit Rivard, Derek MacKenzie, and Mingsheng Ma offered guidance in each of their respective fields, supporting the interdisciplinary nature of the project and my learning experience. Lastly, I am forever indebted to my family and friends, especially my labmate turned graduate student mentor and friend Heather Mosher, for the perpetual emotional support I received throughout my entire graduate school experience. Financial support was provided through Alex Wolfe's NSERC funding.

TABLE OF CONTENTS

LIST OF TABLES

LIST OF FIGURES

CHAPTER 1: INTRODUCTION

1.1. Preamble

Public awareness and opinion towards wildfire activity has grown significantly in recent decades as the intimate connections between fire and climate change impose themselves on the national and international stage. Advances in wildfire prediction and further understanding of the ecological importance of fire have refined the perception of wildfires and reversed policy from complete suppression to more natural management strategies. However, climate change threatens to challenge our current understanding of natural fire processes.

The response of wildfire events to climate change is of utmost importance as we enter a new climate regime, particularly given predictions of increased fire frequency and intensity (Millspaugh *et al.*, 2000; Higuera *et al.*, 2010; Westerling *et al.*, 2011). To successfully manage the future of our forests, we must first attempt to understand the dynamics between vegetation and fire under previous climate systems. Though numerous proxies offer insight into paleofire activity, sedimentary charcoal is the most temporally extensive, enabling the direct reconstruction of fire events on annual to millennial timescales (Whitlock & Larsen, 2001; Conedera *et al.*, 2009; Mooney & Tinner, 2011). However, protocols developed for fossil charcoal analysis lack uniform methodological standardization, which often plagues paleofire reconstructions. Furthermore, the density of sites investigated is often limited by the time-consuming nature of generating fire histories. Because the analysis of long-term fire frequency from sedimentary archives is critical to the understanding of forest dynamics, there is a continuous need to refine methodologies used to reconstruct fire frequency and intensity. Recent advances in the application of spectroscopy in

the environmental sciences present an opportunity to develop remote sensing techniques for quantifying charcoal concentrations from the sedimentary record in a quicker, non-destructive manner.

This chapter reviews current paleoanthracologic techniques, that is, methods employed for sedimentary charcoal quantification. Subsequent sections briefly outline fundamental spectroscopic principles and their environmental applications while detailing the potential benefits and implications of quantitatively measuring charcoal concentrations from lacustrine sediments using Visible Near Infrared (VNIR) absorption spectroscopy. Finally, an overview of the thesis' organization is presented.

1.2. Previous approaches to sedimentary charcoal analysis

Charcoal is a direct indicator of fire activity, as it is formed during the partial combustion of organic matter in oxygen-limited conditions (Clark, 1984; Braadbaart & Poole, 2008; Mooney & Tinner, 2011). Resistance to chemical, biological, and physical deterioration allows charcoal to persist in the sedimentary record as well as withstand numerous laboratory procedures including acid digestion (Conedera *et al.*, 2009; Mooney & Tinner, 2011). Since the establishment of microscopic charcoal studies by Iversen (1941), subsequent research has revealed the applicability of sedimentary charcoal archives as temporally extensive environmental indicators, lending themselves to numerous quantification approaches (Conedera *et al.*, 2009). A brief examination of traditional charcoal analysis techniques follows with commentary on the benefits and challenges that inherently accompany each method. The paleoecological proxies examined include microscopic and macroscopic charcoal from sedimentary records. Although also significant to paleofire studies, dendrochronologic fire scar evidence, black carbon pyrogenic records, and

sedimentary fusain archives are beyond the scope of this review.

Lake, soil, and peat deposits preserve the terrestrial sedimentary charcoal record. Lacustrine sediments are the preferred terrestrial charcoal archive for paleofire studies given that their relatively larger watersheds record more spatially extensive signals. Furthermore, lake sediments largely circumvent problems associated with the susceptibility of peat and soil to repeated burnings, charcoal vertical remobilization, and difficulties in accurate dating (Tolonen, 1983; Conedera *et al.*, 2009). Charcoal concentrations are quantified through optical microscopy counting procedures, enumerating the particle count, area, mass, volume, or proportion of charcoal at each stratigraphic interval (Clark, 1982; Whitlock & Larsen, 2001; Mooney & Tinner, 2011). Uniform standardization of units and methods has yet to be established, requiring *post hoc* data transformations to compare study results for regional and global trends from charcoal databases (Power *et al.*, 2010; Mooney & Tinner, 2011).

Other analytical protocols include the charcoal size classification scheme, which divides charcoal into macroscopic (size fraction > 100 μm) and microscopic (size fraction < 100 μm) classes. Particle transport mechanics presume macroscopic charcoal derives from an immediate, local source area as large particles have low probability of extensive transport distance; conversely, microscopic charcoal originates from farther, extra-local (outside watershed), and regional source areas (Clark, 1988a, 1988b; Whitlock & Millspaugh, 1996; Carcaillet *et al.*, 2001; Tinner *et al.*, 2006). Calibration studies generally validate these assumptions, concluding that macroscopic charcoal settles within a few hundred meters of a fire event while aeolian processes transport microscopic particles 20 to 100 km (Clark, 1988a; Millspaugh & Whitlock, 1995; Tinner *et al.*, 1998; Conedera *et al.*, 2009). Complicating charcoal transport distance assumptions, kilometer-scale transport of centimeter-size charcoal particles

from intense crown fires has been confirmed by both modeling studies and field observations (Pisaric, 2002; Tinner *et al.*, 2006; Peters & Higuera, 2007; Conedera *et al.*, 2009).

Fire dynamics and watershed characteristics dictate charred particle deposition. Fire studies in the western United States indicate sedimentary archives preferentially preserve artifacts of infrequent, high-intensity fires opposed to frequent, lower-intensity ground fires. However, a lag often persists between distinct fire events and charcoal deposition into the sedimentary record due to watershed geomorphology, runoff and drainage patterns, transport mechanisms, and size of charred particles (Whitlock & Larsen, 2001; Conedera *et al.*, 2009; Mooney & Tinner, 2011). Figure 1.1 visually demonstrates the inherent impediments to which charcoal particles are subjected, often precluding idealized depositional scenarios. Delayed charcoal deposition distorts information from the fire itself and often better reflects watershed dynamics, complicating efforts to determine paleofire size and intensity from sedimentary charcoal records.

Regardless of disagreement concerning size fraction transport distance and deposition mechanics of charcoal, sediment layers containing higher charcoal concentrations, or fluxes, are interpreted as direct evidence of fire events. Post-fire deposition of charcoal stored in the watershed often leads to sedimentary archives reflecting continuous charcoal accumulation, even in the most infrequently burning fire regimes. Researchers attribute the apparently continuous deposition of charcoal to biomass changes, depositional processes, bioturbation, sedimentation rates, and reworking from mass-wasting events (Millspaugh & Whitlock, 1995; Long *et al.*, 1998; Carcaillet *et al.*, 2001; Higuera *et al.*, 2010). Work continues on the establishment of uniform *post hoc* thresholds aimed to distinguish discrete fire events, or signals, from the continuously present background charcoal, or noise (Higuera *et al.*, 2007, 2010). Peaks above

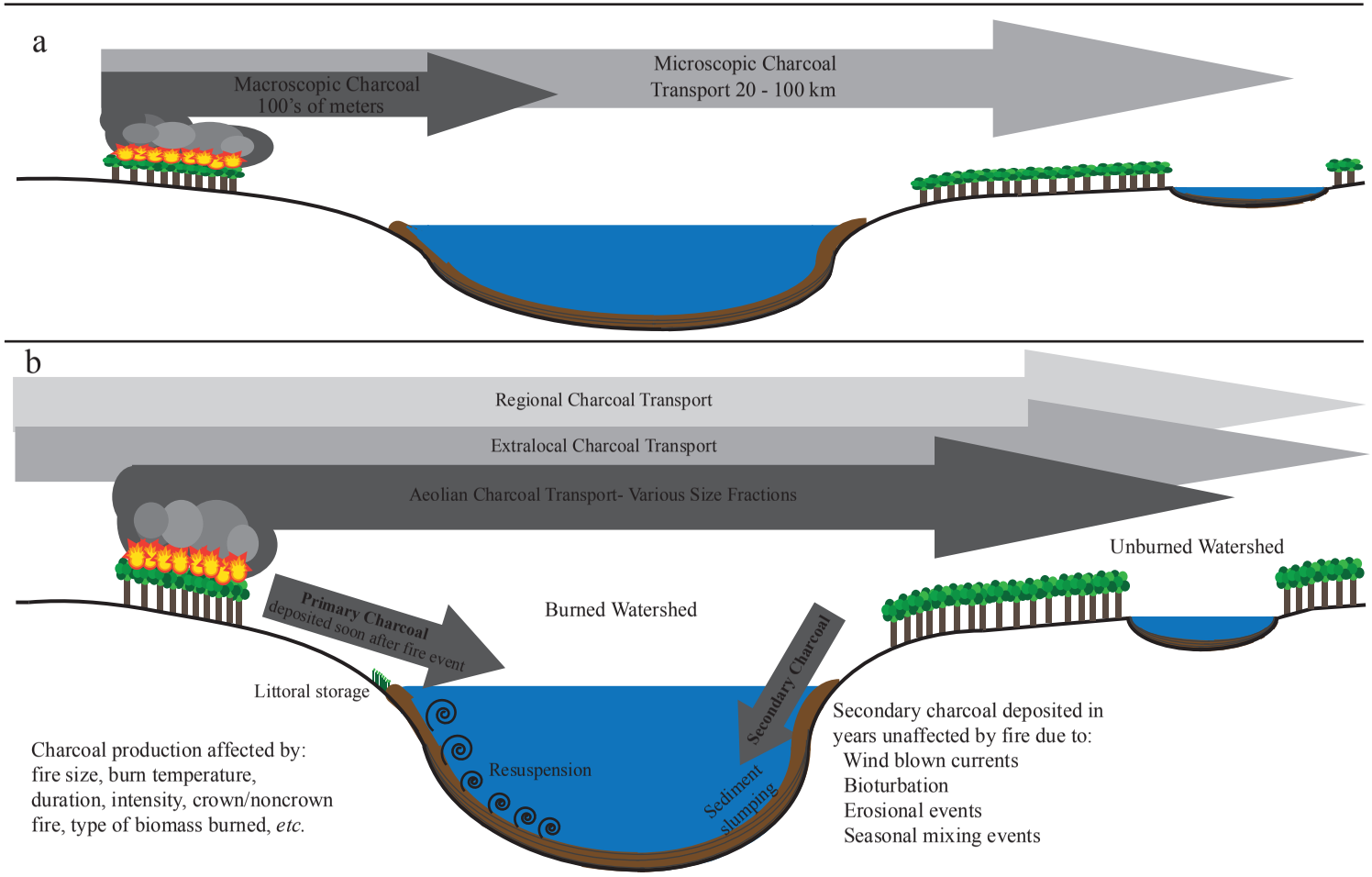

Figure 1.1. Charcoal deposition scenarios (Whitlock & Larsen, 2001; Conedera *et al.*, 2009). An ideal depositional scenario (a) *versus* complications present in a realistic charcoal depositional situation (b).

an established threshold value represent individual fire events or multiple fires occurring during a short time span. Further, consideration of sedimentation rate and chronological control must be taken into account because their effects on peak size and time series resolution considerably influence statistical treatments for peak identification and paleofire interpretation (Millspaugh, 1997; Long *et al.*, 1998; Mohr *et al.*, 2000; Whitlock & Larsen, 2001).

Laboratory procedures for charcoal quantification depend upon geographic scale of interest (i.e. microscopic or macroscopic size fraction for regional or local signals, respectively). Table 1.1 identifies key benefits and limitations associated with the different charcoal quantification methods. Even where standardized laboratory techniques exist (e.g. pollen slide preparation), fire reconstructions from the same sediment core can vary depending on the exact laboratory and data manipulation protocols used. Irrespective of technique utilized, MacDonald *et al.* (1991) found none of the previous methods discussed match the dendrochronologic fire scar record perfectly, raising the question: does the charcoal record appropriately reflect fire history? To circumvent misinterpretation of purely charcoal-based fire histories and produce more compelling reconstructions, pollen data, sedimentological evidence, dendrochronologic fire scar records, and historical accounts typically bolster the sedimentary charcoal record (Meyer *et al.*, 1995; Whitlock & Larsen, 2001; Asselin & Payette, 2005; Conedera *et al.*, 2009). Though corroboration of datasets serves as a multiproxy validation for fire events, these additional methods further slow the generation of realistic fire histories.

Despite the numerous error sources and uncertainties inherent to current sedimentary charcoal quantification techniques, paleofire reconstructions are proving increasingly relevant to forest management in a warming climate, and thus necessitate an objective, automated protocol for the impartial, continuous

Table 1.1. Traditional charcoal quantification techniques (Whitlock & Larsen, 2001; Conedera *et al.*, 2009; Mooney & Tinner, 2011).

Technique	Charcoal Size Class	Geographic Scale	Temporal Resolution	Benefits	Limitations	Examples
Pollen Slide	Microscopic	Indefinite source area, assumed regional	Centennial to millennial	Simultaneous pollen and charcoal analysis and trend cross-referencing for fire regime, biomass, and climate changes	Charcoal particle fragmentation during chemical processing, misrepresentation of size fractions Seiving excludes particles < 10 µm and > 200 µm- ignores potential paleofire information Time intensive preparation prevents continuous sampling intervals	Iversen, 1941; R.L. Clark, 1982; Patterson *et al.*, 1987; MacDonald, 1989
Computer image analysis	Microscopic and macroscopic	Indefinite source area, assumed regional	Centennial to millennial	Speeds particle counting process	Misidentify opaque minerals as charcoal increases data errors Underestimates charcoal quantities compared to optical methods	MacDonald *et al.*, 1991; Clark & Hussey, 1996; Daniau *et al.*, 2004
Sieving	Macroscopic	Local (within watershed) and extralocal	Decadal to millennial	Economical, relatively quick laboratory procedure Typical sampling intervals of 1 cm allow continuous records and fire frequency analysis	No standardization of minimum particle diameter or sample size, affects reproducibility of results	Millspaugh *et al.*, 2000; Brunelle *et al.*, 2005; Higuera *et al.*, 2010; Whitlock *et al.*, 2012
Petrographic thin section	Macroscopic	Local (within watershed) and extralocal	Annual to millennial	Higher temporal resolution, annual precision possible on varved sediments	Expensive, labor intensive, and time consuming Varved samples atypical	J.S. Clark, 1988; Anderson & Smith, 1997
Chemical digestion	None	Unknown	Decadal to millennial	Low charcoal levels detectable	Destructive methodology Notably different results compared to other techniques	Winkler, 1985; Laird & Campbell, 2000

assessment of sedimentary records. To this problem we suggest the use of spectroscopy, an intrinsically unbiased measurement technique that has experienced rapid development in recent decades, often revealing diverse and unforeseen applications to various disciplines.

1.3. Environmental spectroscopy

Spectroscopy analyzes the interaction of electromagnetic radiation with solids, liquids, and gases as a function of wavelength to distinguish chemical compositions and quantify constituents (Hunt, 1982; Clark, 1999). Environmental spectroscopy primarily utilizes the visible (350 – 700 nm) to near infrared (701 – 2500 nm) region of the electromagnetic spectrum, as this range is highly sensitive to elemental electronic and vibrational energy changes (Hunt, 1982). These changes reflect unique patterns that may be used to discriminate materials based on molecular bonding differences (Parish, 2011). Due to its inherent scalability, spectroscopy is becoming increasingly beneficial to the environmental and earth sciences for analyzing global scale features from satellite imagery down to identifying crystallographic imperfections on specific mineral samples.

Spectral indices of soil type, geologic units, vegetation cover, and burned land discrimination are widely employed to remotely monitor terrestrial changes from satellite imagery (Goetz & Rowan, 1981; Viedma *et al.*, 1997; Chuvieco *et al.*, 2002; Smith *et al.*, 2010). Studies of basin-scale shifts in biomass, evident by the optical properties of chlorophyll *a* (e.g. Cózar *et al.*, 2012), and real-time field analyses of Cyanobacteria concentrations (e.g. Randolph *et al.*, 2008) reveal the quantification power and scalability of spectroscopy in biogeochemistry. Numerous research groups investigate the utility and sensitivity of spectral burn indices for charcoal quantification and post-wildfire severity mapping (Chuvieco *et al.*, 2002, 2006; Kokaly *et al.*, 2007; Smith *et al.* 2010).

At finer scales, paleolimnologic efforts concerning the calibration and spectroscopic measurement of suspended minerals and nutrients (*e.g.* carbon, carbonate, nitrogen, phosphorus, and chlorophyll), diatoms, tephra, and other measures of lake productivity and environmental indicators speed the efficiency of sediment analyses and help infer past climate changes (Malley *et al.*, 1996, 1999, 2000; Rosén *et al.*, 2000; Michelutti *et al.*, 2005, 2010; Wolfe *et al.*, 2006; Inagaki *et al.*, 2012). Soil science has also embraced spectroscopy, remotely sensing various soil properties and conducting quality assessments (e.g. Viscarra Rossel *et al.*, 2006; Cécillon *et al.*, 2009), quantifying carbon and charcoal (e.g. Cozzolino & Móron, 2006; Reeves *et al.*, 2007; Bellon-Maurel & McBratney, 2011), and assessing charcoal sources and burn temperature (*e.g.* Guerrero *et al.*, 2007; Arcenegui *et al.*, 2008; Monteiro *et al.*, 2010). The above-mentioned studies present only a brief overview of spectroscopic applications for environmental purposes, but set the stage for paleofire applications from lacustrine sediments.

From the basic principles of spectroscopy and prior research available, the opacity of pyrogenic carbon amplifies absorbance spectra that evolve with increasing charcoal concentration, yielding detectable spectroscopic patterns in the VNIR bands. These absorption features lend themselves to modeling and calibration, with the potential to indirectly assess the total percent charcoal content in sedimentary materials. It is this relationship between measured absorbance and charcoal concentration, previously unexploited for paleolimnologic applications, that enables spectroscopy to quantify charcoal included in lake core sediments and ultimately be developed into a predictive tool for paleofire reconstructions.

1.4. Spectroscopy for charcoal quantification

Spectroscopic analysis has the potential to improve current charcoal

quantification techniques and decipher paleofire reconstructions. As evidenced by the numerous drawbacks of optical counting procedures from pollen slide and various other quantification processes, current paleoanthracologic methodologies necessitate the automation and impartial techniques conveniently offered by spectroscopy.

1.4.1. Spectroscopic benefits to paleoanthracology

Spectroscopy is intrinsically non-destructive, so the same samples analyzed spectroscopically may be utilized again for other laboratory procedures. This quality benefits the examination of precious or archived specimens, facilitating multiple analyses in a sequence of non-destructive to destructive assays. Spectroscopy presents a more inclusive charcoal counting procedure, comprising all charcoal particles regardless of their size. Including all pyrogenic fractions as a composite is currently impossible due to sample preparation differences between macroscopic and microscopic fractions for optical analyses, as well as impractical because of the time required to enumerate enough charcoal particles necessary to sufficiently represent all size ranges from individual samples. Although macroscopic charcoal sieving methods allow for single, centimeter-scale sampling intervals, lengthy pollen slide preparations and time investment in microscopy generally preclude continuous sampling of the microscopic size fraction (Whitlock & Larsen, 2001; Conedera *et al.*, 2009; Mooney & Tinner, 2011). Continuous records are essential for explicit paleofire frequency analysis, and spectroscopy is capable of providing this benefit in a relatively rapid manner. Thus, the advantages spectroscopy offers to charcoal quantification may quickly and efficiently elucidate finer scale changes in paleofire occurrence and fire regime patterns, thereby increasing sample throughput and ultimately assisting future wildfire predictions.

1.4.2. Potential drawbacks of spectroscopic applications to paleoanthracology

Foreseeable problems utilizing spectroscopy for charcoal quantification include fire scale qualification, particle size distortions to spectral absorbance patterns, and model applicability to multiple study areas. Distinguishing local scale fires will unlikely remain feasible through spectroscopic analysis due to the local *versus* regional event classification scheme based on charcoal particle size fractions. Spectroscopy is unable to discriminate particle size fractions, which may ultimately prove either beneficial or disadvantageous to the method's overall utility, depending on individual study goals. Spectroscopically derived charcoal accumulation estimations will thus present continuous data on total included charcoal, rather than microscopic or macroscopic assessments of charcoal at discrete sampling intervals.

Though spectroscopy is incapable of reporting size fractions, differences in particle size affect spectral signatures (Clark & Roush, 1984; Hapke, 1993; Clark, 1999). Beer's Law dictates larger grains absorb more photons while smaller grains present more surfaces for reflection, allowing greater scattering of energy and higher reflectance (Clark, 1999). Thus, sediments dominated by larger charcoal particles risk recording higher absorbance values compared to samples with equally abundant charcoal present at smaller size fractions. Such an effect must be accounted for in quantification studies and techniques to adjust results accordingly require development (i.e. sieving protocols).

Lastly, it is currently unclear as to whether calibration models of sediment-charcoal spectroscopic interactions can be similarly applied to sediments from different lakes without recalibration. Multi-lake studies to determine a calibration model's ability to accurately predict charcoal concentration from sediments of different origin require investigation. One may presume that baseline sediment spectral dissimilarities exist between various lakes due to geologic, biologic,

and chemical differences; however, empirical testing of such hypotheses will eventually prove necessary.

Although they are conceptually elegant, spectroscopically-derived charcoal metrics may further complicate attempts to generalize regional and global fire trends through comparative studies. However, the relative ease and low cost with which spectroscopic analyses may be performed on existing samples holds considerable potential to reassess our current understanding of fire regime changes at various temporal and spatial scales, thus offsetting problems concerning their direct comparison to optically counted microscopic results.

1.5. Progression of chapters

This thesis seeks to establish a novel method that uses environmental spectroscopy to develop a viable paleofire proxy from lacustrine sediments. Subsequent chapters address the calibration (Chapter 2) and application (Chapter 3) of a spectroscopic procedure for sedimentary charcoal quantification and paleofire reconstruction. These chapters are presented as stand-alone manuscripts with the ultimate goal of publication as journal articles. Chapter 4 discusses the broader conclusions of the study implied by the preceding chapters, highlights strengths and weaknesses of the approach, and outlines directions for future research.

1.6. References

Arcenegui, V., Guerrero, C., Mataix-Solera, J., Mataix-Beneyto, J., Zornoza, R., Morales, J., Mayoral, A.M. 2008. The presence of ash as an interference factor in the estimation of the maximum temperature reached in burned soils using near-infrared spectroscopy (NIR). Catena 74: 177-184.

Asselin, H. & Payette, S. 2005. Detecing local-scale fire episodes on pollen slides. Review of Palaeobotany and Palynology 137: 31-40.

Bellon-Maurel, V. & McBratney, A. 2011. Near-infrared (NIR) and mid-infrared (MIR) spectroscopic techniques for assessing the amount of carbon stock in soils – Critical review and research perspectives. Soil Biology & Biochemistry 43: 1398-1410.

Braadbaart, F. & Poole, I. 2008. Morphological, chemical and physical changes during charcoalification of wood and its relevance to archaeological contexts. Journal of Archaeological Science 35: 2434-2445.

Carcaillet, C., Bouvier, M., Fréchette, B., Larouche, A.C., Richard, P.J.H. 2001. Comparison of pollen-slide and sieving methods in lacustrine charcoal analyses for local and regional fire history. The Holocene 11: 467-476.

Cécillon, L., Cassange, N., Czarnes, S., Gros, R., Vennetier, M., Brun, J. 2009. Predicting soil quality indices with near infrared analysis in wildfire chronosequence. Science of the Total Environment 407: 1200-1205.

Chuvieco, E., Martin, M.P., Palacios, A. 2002. Assessment of different spectral indicies in the red-near-infrared spectral domain for burned land discrimination. International Journal of Remote Sensing 23: 5103-5110.

Chuvieco, E., Riaño, D., Danson, F.M., Martin, P. 2006. Use of a radiative transfer model to simulate the postfire spectral response to burn severity. Journal of Geophysical Research 111: G04S09 doi:10.1029/2005JG000143.

Clark, J.S. 1988a. Particle Motion and the Theory of Charcoal Analysis: Source Area, Transport, Deposition, and Sampling. Quaternary Research 30: 67-80.

Clark, J.S. 1988b. Stratigraphic charcoal analysis on petrographic thin sections: application to fire history on Northwestern Minnesota. Quaternary Research 30: 81-91.

Clark, R.L. 1982. Point count estimation of charcoal in pollen preparations and thin sections of sediment. Pollen et Spores 24: 523-535.

Clark, R.L. 1984. Effects on charcoal of pollen preparation procedures. Pollen et Spores 2: 559-576.

Clark, R.N. 1999. Spectroscopy of Rocks and Minerals, and Principles of Spectroscopy. In Manual of Remote Sensing: Volume 3 Remote Sensing for the Earth Sciences; Rencz, A.N. John Wiley and Sons, New York: 3-58.

Clark, R.N. & Roush, T.L. 1984, Reflectance spectroscopy: Quantitative analysis techniques for remote sensing applications, Journal of Geophysical Research 89: 6329- 6340.

Conedera, M., Tinner, W., Neff, C., Meurer, M., Dickens, A.F., Krebs, P. 2009. Reconstructing past fire regimes: methods, applications, and relvance to fire management and conservation. Quaternary Science Reviews 28: 555-576.

Còzar, A., Bruno, M., Bergamino, N., Ubeda, B., Bracchini, L., Dattilo, A.M., Loiselle, S.A. 2012. Basin-scale control on the phytoplankton biomass in Lake Victoria, Africa. PLoS ONE 7: e29962. Doi:101371/journal.pone.0029962.

Cozzolino, D. & Morón, A. 2006. Potential of near-infrared reflectance spectroscopy and chemometrics to predict soil organic carbon fractions.

Soil & Tillage Research 85: 78-85.

Daniau, A.L., Sánchez-Goñi, M.F., Beaufort, L., 2004. Fire regime and climate variability over the last 140,000 years in South Western Iberia. In: D'Andria, F., Fiorentino, G., Magri, D. (Eds.), International Meeting of Anthracology, Charcoals from the Past: Cultural and Palaeoenvironmental Implications. Universita` di Lecce, Scuola di specializzazione in Archeologia, Convento dei Domenicani Cavallino, Lecce (Italy).

Goetz, F.H. & Rowan, L.C. 1981. Geologic remote sensing. Science 211: 781-791.

Guerrero, C., Mataix-Solera, J., Arcenegui, V., Mataix-Beneyto, J., Gómez, I. 2007. Near-infrared spectroscopy to estimate the maximum burned temperatures reached on burned soils. Soil Science Society of America Journal 71: 1029-1037.

Hapke, B. 1993. Introduction to the Theory of reflectance and Emittance Spectroscopy, Cambridge University Press, New York.

Higuera, P.E., Peters, M.E., Brubaker, L.B., Gavin, D.G. 2007. Understanding the origin and analysis of sediment–charcoal records with a simulation model. Quaternary Science Reviews 26: 1790-1809.

Higuera, P.E., Whitlock, C., Gage, J.A. 2010. Linking tree-ring and sediment-charcoal records to reconstruct fire occurrence and area burned in subalpine forests of Yellowstone National Park, USA. The Holocene 21: 327-341.

Hunt, G.R. 1982. Spectroscopic properties of rocks and minerals. In: Carmichael, R.S. (Ed.), Handbook of Physical properties of rocks, Volume 1. CRC Press: 295-385.

Inagaki, T., Shinozuka, Y., Yamada, K., Yonenobu, H., Hayashida, A., Tsuchikiawa, S., Yoshida, A., Hoshino, Y., Gotanda, K., Yasuda, Y. 2012.

Rapid prediction of past climate condition from lake sediments by near-infrared (NIR) spectroscopy. Applied Spectroscopy 66: 673-679.

Iversen, J. 1941. Landnam i Danmarks stenalder (Land occupation in Denmark's Stone Age). Danmarks Geologiske Undersogelse 66: 1-68.

Kokaly, R.F., Rockwell, B.W., Haire, S.L., King, T.V.V. 2007. Characterization of post-fire surface cover, soils, and burn severity at the Cerro Grande Fire, New Mexico, using hyperspectral and multispectral remote sensing. Remote Sensing of Environment 106: 305-325.

Long, C.J., Whitlock, C., Bartlein, P.J., Millspaugh, S.H. 1998. A 9000-year fire history from the Oregon Coast Range, based on a high-resolution charcoal study. Canadian Journal of Forest Research 28: 774-787.

MacDonald, G.M., 1989. Postglacial palaeoecology of the subalpine forest-grassland ecotone of southwestern Alberta: new insights on vegetation and climate change in the Canadian Rocky Mountains and adjacent foothills. Palaeogeography, Palaeoclimatology, Palaeoecology 73: 155–173.

MacDonald, G.M., Larsen, C.P.S., Szeicz, J.M., Moser, K.A. 1991. The reconstruction of boreal forest fire history from lake sediments: a comparison of charcoal, pollen, sedimentological, and geochemical indices. Quaternary Science Review 10: 53-71.

Malley, D., Williams, P.C., Stainton, M. 1996. Rapid measurement of suspended C, N, and P from Precambrian shield lakes using near-infrared reflectance spectroscopy. Water Research 30: 1325-1332.

Malley, D., Lockhart, L., Wilkinson, P., Hauser, B. 2000. Determination of carbon, carbonate, nitrogen, and phosphorous in freshwater sediments by near-infrared reflectance spectroscopy: rapid analysis and a check on conventional analytical methods. Journal of Paleolimnology 24: 415-425.

Malley, D., Rönicke, H., Findlay, D.L., Zippel, B. 1999. Feasibility of using near-

infrared reflectance spectroscopy for the analysis of C, N, P, and diatoms in lake sediments. Journal of Paleolimnology 21: 295-306.

Meyer, G.A., Wells, S.G., Jull, A.J.T. 1995. Fire and alluvial chronology in Yellowstone National Park: Climatic and intrinsic controls on Holocene geomorphic processes. Geological Society of America Bulletin 107: 1211-1230.

Michelutti, N., Blais, J.M., Cumming, B.F., Paterson, A.M., Rühland, K., Wolfe, A.P., Smol, J.P. 2010. Do spectrally inferred determinations of chlorophyll a reflect trends in lake trophic status? Journal of Paleolimnology 43: 205-217.

Michelutti, N., Wolfe, A.P., Vinebrooke, R.D., Rivard, B., Briner, J.P. 2005. Recent primary production increases in arctic lakes. Geophysical Research Letters 32: L19715, doi:10.1029/2005GL023693.

Millspaugh, S. H. 1997. Late-glacial and Holocene variations in fire frequency in the Central Plateau and Yellowstone-Lamar Provinces of Yellowstone National Park. Ph.D. dissertation, University of Oregon, Eugene, OR.

Millspaugh, S.H. & Whitlock, C. 1995. A 750-year fire history based on lake sediment records in central Yellowstone National Park. USA. The Holocene 5: 283-292.

Millspaugh, S.H., Whitlock, C., Bartlein, P.J. 2000. Variations in fire frequency and climate over the past 17 000 yr in central Yellowstone National Park. Geology 28: 211-214.

Mohr, J.A., Whitlock, C., Skinner, C.J. 2000. Postglacial vegetation and fire history, eastern Klamath Mountains. California. The Holocene 10: 587-601.

Monteiro, T.C., da Silva, R.V., Lima, J.T., Hein, P.R.G., Napoli, A. 2010. Use of near infrared spectroscopy to distinguish carbonization processes and

charcoal sources. Cerne, Lavras 16: 381-390.

Mooney, S.D. & Tinner, W. 2011. The analysis of charcoal in peat and organic sediments. Mires and Peat 7: 1-18.

Parish, R.M. 2011. The application of visible/near-infrared reflectance (VNIR) spectroscopy to chert: a case study from the Dover Quarry sites, Tennessee. Geoarchaeology 26: 420-439.

Peters, M.E., Higuera, P.E. 2007. Quantifying the source area of macroscopic charcoal with a particle dispersal model. Quaternary Research 67: 304-310.

Pisaric, M.F.J. 2002. Long-distance transport of terrestrial plant material by convection resulting from forest fires. Journal of Paleolimnology 28: 349-354.

Power, M.J., Marlon, J.R., Bartlein, P.J., Harrison, S.P. 2010. Fire history and the Global Charcoal Database: A new tool for hypothesis testing and data exploration. Palaeogeography, Palaeoclimatology, Palaeoecology 291: 52-59.

Randolph, K., Wilson, J., Tedesco, L., Lin, L., Pascual, D.L., Soyeux, E. 2008. Hyperspectral remote sensing of cyanobacteria in turbid productive water using optically active pigments, chlorophyll *a* and phycocyanin. Remote Sensing of Environment 112: 4009-4019.

Reeves III, J.B. McCarty, G.W., Rutherford, D.W., Wershaw, R.L. 2007. Near infrared spectroscopic examination of charred pine wood, bark, cellulose and lignin: implications for the quantitative determination of charcoal in soils. Journal of Near Infrared Spectroscopy 15: 307-315.

Rosén, P., Dåbakk, E., Renberg, I., Nilsson, M., Hall, R. 2000. Near-infrared spectrometry (NIRS): a new tool for inferring past climatic changes from lake sediments. The Holocene 10: 161-166.

Smith, A.M.S., Eitel, J.U.H., Hudak, A.T. 2010. Spectral analysis of charcoal on soils: implications for wildland fire severity mapping methods. International Journal of Wildland Fire 19: 976-983.

Tinner, W., Conedera, M., Ammann, B., Gäggeler, H.W., Gedye, S., Jones, R., Sägesser, B. 1998. Pollen and charcoal in lake sediments compared with historically documented forest fires in southern Switzerland since AD 1920. Holocene 8: 31-42.

Tinner, W., Hofstetter, S., Zeugin, F., Conedera, M., Wohlgemuth, T., Zimmermann, L., Zweifel, R. 2006. Long-distance transport of macroscopic charcoal by an intensive crown fire in the Swiss Alps – implications for fire history reconstruction. The Holocene 16: 287-292.

Tolonen, K. 1983. The post-glacial fire record. In The Role of Fire in Northern Circumpolar Ecosystems; Wein, R.W., MacLean, D.A. John Wiley & Sons, New York: 21-44.

Viedma, O., Melià, J., Segarra, D., García-Haro, J. 1997. Modeling rates of ecosystem recovery after fires using Landsat TM data. Remote Sensing of Environment 61: 383-398.

Viscarra Rossel, R.A., Walvoort, D.J.J., McBratney, A.B., Janik, L.J., Skjemstad, J.O. 2006. Visible, near infrared, mid infrared or combined diffuse reflectance spectroscopy for simultaneous assessment of various soil properties. Geoderma 131: 59-75.

Westerling, A.L., Turner, M.G., Smithwick, E., Romme, W.H., Ryan, M.G. 2011. Continued warming could transform greater Yellowstone fire regimes by mid-21st century. Proceedings of the National Academy of Sciences of the United States of America 108: 13165-13170.

Whitlock, C. & Larsen, C. 2001. Charcoal as a fire proxy. In Tracking Environmental Change Using Lake Sediments: Volume 3 Terrestrial,

Algal, and Siliceous indicators; Smol, J.P., Birks, H.J.B., and Last. W.M. Kluwer Academic Publishers, Dordrecht: 75-97.

Whitlock, C. & Millspaugh, S.H. 1996. Testing the assumptions of fire-history studies: An examination of modern charcoal accumulation in Yellowstone National Park, USA. Holocene 6: 7-16.

Wolfe, A.P., Vinebrooke R.D., Michelutti N., Rivard B., Das B. 2006. Experimental calibration of lake-sediment spectral reflectance to chlorophyll a concentrations: methodology and paleolimnological validation. Journal of Paleolimnology 36: 91-100.

CHAPTER 2

A HYPERSPECTRAL METHODOLOGY TO INFER CHARCOAL CONCENTRATIONS FROM LACUSTRINE SEDIMENTS

2.1. Introduction

With increased concern over future climate scenarios and their resultant effects on natural resources, forest managers are increasingly looking to the paleoecological community for answers regarding the frequency and ecological response of forest fires over time, and moreover their long-term relationship to Holocene climate change (Shoennagel *et al.*, 2004; Whitlock *et al.*, 2008; Bowman *et al.*, 2009; Conedera *et al.*, 2009; Flannigan *et al.*, 2009; Marlon *et al.*, 2010, 2012; Westerling *et al.*, 2011). The sedimentary record of lakes offers a temporally continuous archive of fire-climate-vegetation dynamics. However, current sediment paleofire analyses employ various analytical protocols, each with their own strengths and weaknesses (Laird & Campbell, 2000; Carcaillet *et al.*, 2001; Whitlock & Larsen, 2001; Enache & Cummings, 2006; Conedera *et al.*, 2009; Mooney & Tinner, 2011), but universally requiring large investments of time for microscopic determinations of charcoal abundance in the sediment record. Furthermore, comparison of data generated by different protocols is never straightforward. In response to this situation, we present a novel methodology for sediment charcoal analysis that exploits diffuse reflectance spectroscopy. From the outset, we hypothesized that charcoal should impart opacity to sediments that can be readily detected spectroscopically, and that this signature can be related to the total amount of charcoal present in a given lacustrine sediment matrix. Conceptually, this approach builds on previous applications of environmental spectroscopy in paleoenvironmental reconstruction (Malley *et al.*, 1996, 2000;

Malley, 1998; Rosén *et al.*, 2000; Michelutti *et al.*, 2005, 2010; Wolfe *et al.*, 2006; Rosén & Hammarlund, 2007; Bellon-Maurel & McBratney, 2011).

The Greater Yellowstone Ecosystem (GYE: the 80,000 km^2 contiguous area encompassing Yellowstone National Park, Grand Teton National Park, and the Beartooth Absaroka Wilderness) has a relatively well-understood Holocene fire history based on numerous paleofire analyses using a variety of conventional charcoal quantification techniques (e.g. Romme & Despain, 1989; Millspaugh & Whitlock, 1995; Whitlock & Millspaugh, 1996; Millspaugh *et al.*, 2000; Brunelle *et al.*, 2005; Huerta *et al.*, 2009; Higuera *et al.*, 2010; Whitlock *et al.*, 2012). Alpine lakes in Grand Teton National Park, within the southern sector of the GYE, are excellent beacons for regional paleofire reconstruction, and record major historical events including the extensive (5700 km^2) 1988 Yellowstone National Park wildfires (Whitlock, 1993; Jacobs & Whitlock, 2008; Romme *et al.*, 2011). Alpine lake catchments that are largely above the regional treeline are especially sensitive to extra-local charcoal inputs typically associated with larger regional fire events.

Sediment matrices obtained from two such lakes were used to calibrate the spectroscopic response to incremental additions of charcoal, spanning the full range from pure sediment to pure charcoal. A range of spectral indices, statistical treatments, and data transformations were explored to understand the spectroscopic effects on lake-sediment matrices to varying amounts of charcoal. A calibration was also devised between sediment spectral signatures and total black carbon determined from amended samples using the protocol of Kurth *et al*. (2006).

In developing this new proxy, we aim to reduce human error and data inaccuracies inherent to optical counting procedures, remove fire scale biases associated with size fraction requirements relating to specific laboratory

techniques, and decrease the time investment required to perform charcoal analyses, thus reducing overall laboratory expenses and enabling, for example, stratigraphically continuous analyses. Utilizing environmental spectroscopy, we develop a reliable, non-destructive, and relatively rapid method for sedimentary charcoal quantification and paleofire determination.

2.2. Site and sample descriptions

Sediments were collected from two alpine lakes in Grand Teton National Park in July 2010. Whitebark Moraine Pond (informal name, 43.79° N, 110.79° W; 2800 m asl; area: 0.76 ha; depth: 8 m) is formed by the damming of the upper reaches of Paintbrush Canyon by lateral and recessional moraines, approximately 0.4 km southeast of Holly Lake (Figure 2.1). Ramshead Lake (43.78° N, 110.79° W; 2895 m asl; area: 0.85 ha; depth: 14 m) is situated in Hanging Canyon immediately downstream (300 m) of Lake of the Crags, the headwater (Figure 2.1). Although these lakes have strongly nival hydrological regimes, abundant unvegetated talus, and late-lying snowpacks that may survive cold summers, they also have pronounced differences that are ultimately expressed by sediment lithology.

Whitebark Moraine Pond has a small catchment and does not occupy the main axis of drainage in Paintbrush Canyon; the lake's margin is vegetated, including abundant Whitebark Pine (*Pinus albicaulis*) on all but the western shore, for which the site has been labeled. Consequently, sediments are highly-organic brown gyttja (sapropel) with organic contents >20%.

Ramshead Lake integrates the much larger catchment of the upper Hanging Canyon, including outflow from Lake of the Crags. All drainage in the cirque between Mount St. John and the Rock of Ages, including that from perennial snowpacks, passes through Ramshead Lake prior to dropping

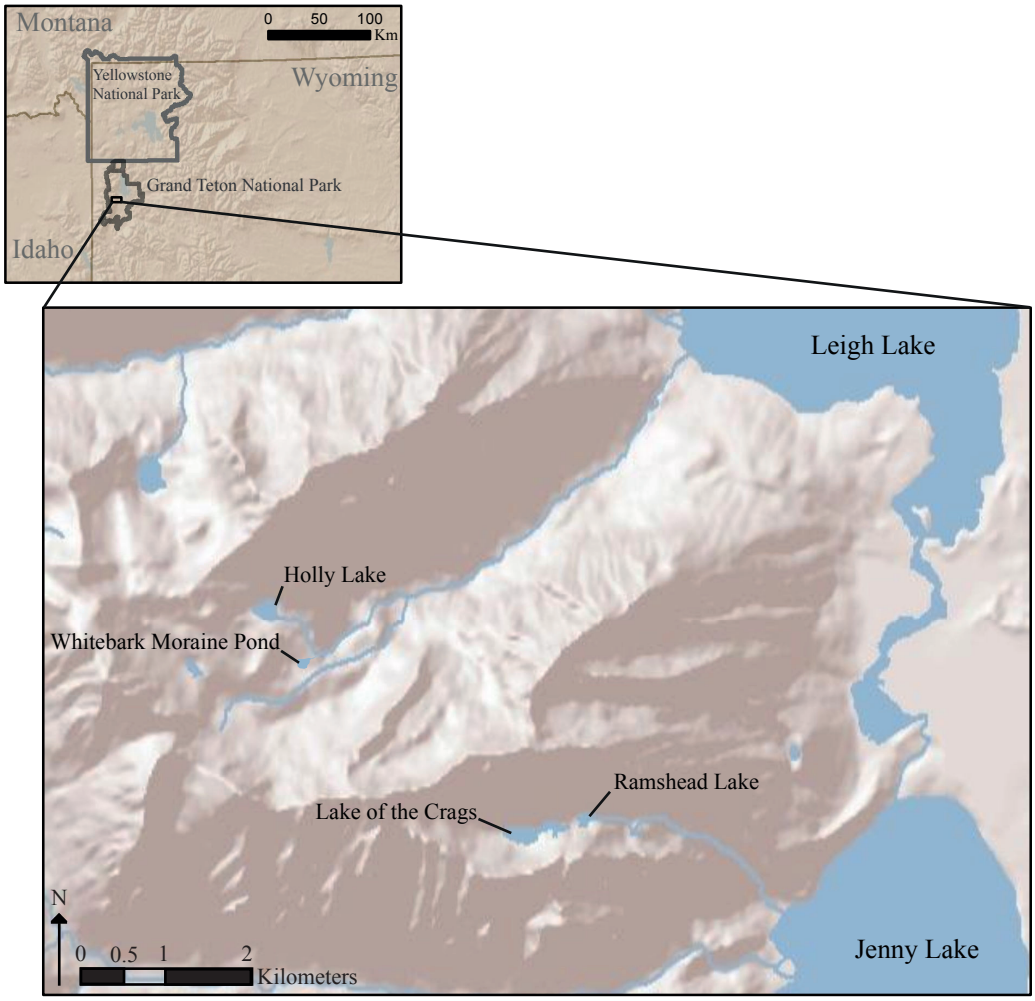

Figure 2.1. Study site map. Regional and detailed site map highlighting Whitebark Moraine Pond and Ramshead Lake within Grand Teton National Park.

precipitously to Jenny Lake, itself defined by a prominent Late Pinedale moraine loop. Ramshead Lake sediments are consequently comprised of more minerogenic grey silt sediments, with <10% organic matter.

2.3. Methodology

2.3.1. Calibration series

Near-surface sediments from both lakes were used as matrices for charcoal amendments. Sediments were collected using a gravity corer (Glew, 1991), thoroughly mixed, and freeze-dried. The modern sediments are presumed to have little significant charcoal given wildfire quiescence in recent years.

The charcoal inoculum was collected from each of the conifer species occurring regionally: Engelmann spruce (*Picea engelmannii*), Lodgepole pine (*Pinus contorta*), Douglas fir (*Pseudotsuga menziesii*), and Whitebark Pine. Charcoals presumably result from the 1988 Yellowstone wildfires. Dried and crushed aliquots of charcoal from each taxon were mixed to 1:1:1:1 ratios. Scanning electron microscope (SEM) images and micrographs of the inoculum display the angularity and color range exhibited by the charcoal fragments (Figure 2.2-3).

Incrementally increasing concentrations of the charcoal standard were added to the sediment matrix of each lake in order to create a mass-ratio dilution series to assess the evolution of spectroscopic signatures in relation to charcoal concentration. Each matrix underwent fourteen dilutions as detailed in Table 2.1. To mitigate absorbance variations due to particle size (shading and other topographic effects), we utilized only the <125 μm sieved fraction for spectroscopy.

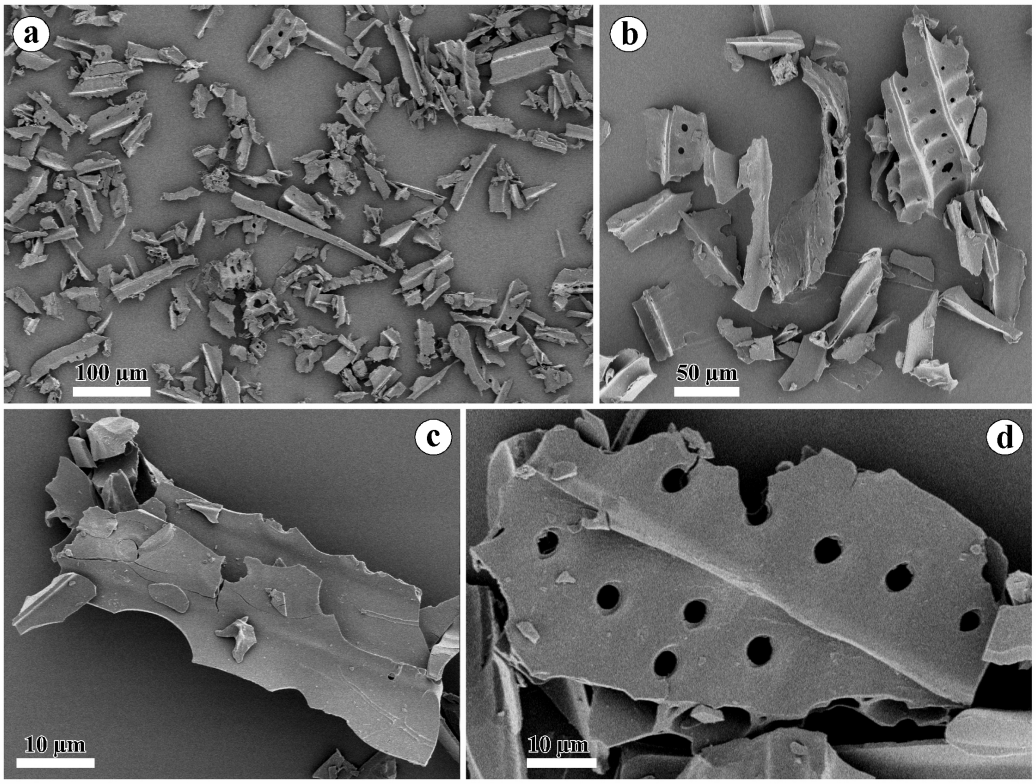

Figure 2.2. Charcoal SEM plate. SEM images of modern charcoal standard (a-d) displaying the angularity and size of charcoal fragments utilized as the dilution series inoculum.

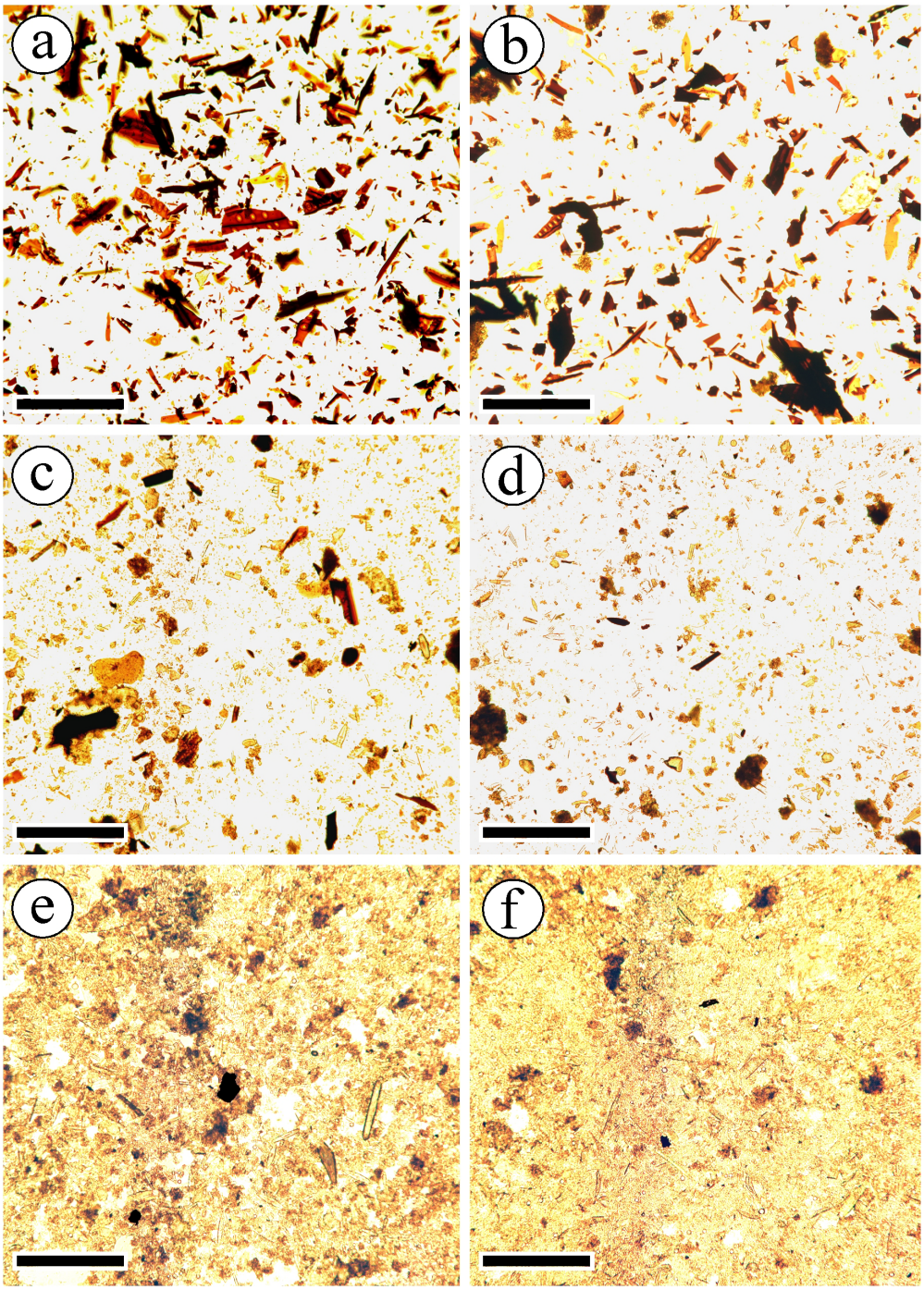

Figure 2.3. Micrographs of charcoal standard. Light micrographs of spiked calibration (a-d) and natural (e-f) samples. Scale bars are 10 µm. Pure charcoal is shown in (a), 50% charcoal in (b), 4% in (c), and 0.5% in (d). In (e) are sediments from 1.75 cm in the Whitebark Moraine Pond gravity core, where charcoal fragments are likely reworked from the 1988 Yellowstone fires. The sample in (f) is from 154.5 cm in the percussion core, corresponding to sediments deposited immediately above the Mazama tephra (see Chapter 4 for details).

Table 2.1. Charcoal calibration series.

Lake	Charcoal mass (mg)	Sediment mass (mg)	Total mass (mg)	Ratio (sed:char)	Charcoal percentage
Whitebark Moraine Pond	225.00	224.90	499.90	1:1	50.00%
	83.30	416.70	500.00	5:1	16.68%
	45.50	450.10	495.60	10:1	9.10%
	31.50	468.80	500.30	15:1	6.30%
	19.20	480.70	499.90	25:1	3.83%
	9.80	490.20	500.00	50:1	1.96%
	6.60	493.40	500.00	75:1	1.32%
	5.00	500.00	505.00	100:1	0.99%
	2.50	500.10	502.60	200:1	0.50%
	1.20	480.00	481.20	400:1	0.25%
	0.80	480.00	480.80	600:1	0.17%
	0.60	480.00	480.60	800:1	0.13%
	0.50	500.00	500.50	1000:1	0.10%
	0.00	500.00	500.00	1:0	0.00%
Ramshead Lake	300.40	300.40	600.80	1:1	50.01%
	83.40	416.70	500.10	5:1	16.66%
	31.50	454.40	499.90	10:1	9.18%
	31.50	468.80	500.30	15:1	6.30%
	19.20	480.90	500.10	25:1	3.84%
	9.80	490.20	500.00	50:1	1.96%
	6.60	493.50	500.10	75:1	1.32%
	5.00	500.10	505.10	100:1	0.99%
	2.50	500.00	502.50	200:1	0.50%
	1.20	480.00	481.20	400:1	0.25%
	0.80	480.10	480.90	600:1	0.17%
	0.60	480.00	480.60	800:1	0.12%
	0.50	500.10	500.60	1000:1	0.10%
	0.00	500.00	500.00	1:0	0.00%
Charcoal standard	500.00	0.00	500.00	0:1	100%

2.3.2. Spectroscopic measurement

Approximately 4 g of each sample were placed in glass scintillation vials for spectroscopic measurements using a Model 6500 series Rapid Content Analyzer (FOSS NIRSystems Inc.) at Queen's University (Kingston, Ontario). The samples were measured for absorbance (A=log(1/reflectance)) across visible to near-infrared wavelengths (400 nm to 2498 nm) at 2 nm intervals. Absorbance values of each sample represent an average of 32 scans. Measurement of the Rapid Content Analyzer ceramic reference panel every four samples prevented spectral data drift throughout the measurement process. Analysis time of each sample, including reference panel adjustments, was approximately one minute.

2.3.3. Calibration models

Measurable patterns in absorbance variations with differing charcoal concentrations required data summation techniques, of which many were employed to produce statistically significant models. Table 2.2 summarizes the highest performing statistical methods relating the absorbance data and the motivation of each attempt. Where necessary to ensure normal distribution during linear regression, spectroscopic data were statistically transformed alternately using $\log_{10}$ transformations as well as first and second derivatives. Subsequent adjusted coefficients of determination (r^2), and the Root Mean Squared Error of Prediction (RMSEP) in the case of Partial Least Squares Regression (PLSR) models, were utilized to assess the performance of each model (Mevik & Wehrens, 2007). RMSEP expresses prediction error in units identical to the unit of measure, thus in charcoal percentages.

Briefly, normalization to unity was used to remove all negative absorbance values within the visible to near infrared (VNIR) spectrum. Area beneath the curve measured peaks in absorbance within known ranges of spectral interest.

Table 2.2. Statistical methods attempted for calibration modeling. All methods are performed on absorbance values where: RED = 626 to 740 nm, NIR = 750 to 1400 nm, and * denotes method performed on normalized absorbance values.

Method	Number	Method details	Reasoning	Sources
Normalization	1	$= \frac{\text{(Sample - Minimum Absorbance)}}{\text{(Maximum - Minimum Absorbance)}}$	Remove negative absorbance values to ease calibration-core comparisons	This study
Area beneath curve	2a	Area calculation (536 to 570 nm) *	Measure dampening of Chlorophyll *a* signal with increased charcoal	Das *et al.*, 2005, Mitchelutti *et al.*, 2005, 2010; Wolfe *et al.*, 2006
	2b	Area calculation (700 to 1850 nm)	Measure area between Chlorophyll *a* band and OH feature	
	2c	Area calculation (1886 to 2000 nm) *	Measure variation in OH feature with increased charcoal	
NDVI	3a	= (NIR - RED) / (NIR + RED)	Spectral index analysis	Smith *et al.*, 2010
	3b	= (NIR - RED) / (NIR + RED) *	Spectral index analysis	
OSAVI	4a	= (NIR - RED) / (NIR + RED + 0.16)	Spectral index analysis	
	4b	= (NIR - RED) / (NIR + RED + 0.16) *	Spectral index analysis	
BAI	5a	$= [(RED_{CHAR} - RED)^2] + [(NIR_{CHAR} - NIR)^2]$	Spectral index analysis	Chuvieco *et al.*, 2002
	5b	$= [(RED_{CHAR} - RED)^2] + [(NIR_{CHAR} - NIR)^2]$*	Spectral index analysis	
Standard deviation	6	$= \frac{\text{(452 nm - 860 nm)}}{\text{(452 nm + 860 nm) *}}$	Compare highest to lowest standard deviation wavelengths	This study
Slope	7	Linear slope coefficient (1500 to 1850 nm)	Allow comparison of unnormalized calibration series to core spectra	This study
PLSR	8a	PLSR on 1st & 2nd derivative (400 – 2498 nm)	PLSR on derivatives to pick up minute spectral feature differences	Malley *et al.*, 1996; Cozzolion & Móron, 2006; Bellon-Maurel & McBratney, 2011
	8b	PLSR on 1st & 2nd derivative (800 – 2498 nm)	" ... " outside visible spectrum	
	8c	PLSR on 1st & 2nd derivative (1000 – 2498 nm)	" ... " outside red overtone zone	
	8d	PLSR on 1st & 2nd derivative (1500 – 2498 nm)	" ... " beyond ~1400 nm OH feature	

The Normalized Difference Vegetation Index (NDVI), Optimized Soil-Adjusted Vegetation Index (OSAVI), and Burn Area Index (BAI) represent spectral indices previously employed in pedologic fire studies (Chuvieco *et al.*, 2002; Smith *et al.*, 2010). Standard deviation and slope analyses are novel methods created specifically for this project. PLSR is an alternative to Principal Component Analysis (PCA) and favored in numerous spectroscopic applications (Malley *et al.*, 1996; Cozzolion & Móron, 2006; Bellon-Maurel & McBratney, 2011). In the case of Whitebark Moraine Pond, the most skilled models were then readjusted and refined to the 0 – 10% charcoal range (instead of 0 – 100%), in order to focus on the lower range of charcoal concentrations anticipated for real-world scenarios and down-core applications from this site (Chapter 3).

Statistical analyses were principally implemented in the R environment (v.2.13.1; R Development Core Team, 2011). We used Spekwin32 version 1.71.6 for spectral visualization and all derivations (Menges, 2011). Both software packages are available for free download online.

2.3.4. KMD carbon calibration

Carbon content was analyzed in selected samples of the charcoal dilution series using a variation of the black carbon protocol of Kurth *et al*. (2006). Briefly, 0.5 g of freeze-dried sample sediment was mixed with 20 mL of 30% H_2O_2 in a 250 mL Erlenmeyer flask. After sitting 4 hours with constant mixing, 10 mL of 1 M HNO_3 is added and allowed to digest for 19 hours. The samples are then heated to 50°C for 4 hours with occasional swirling and again allowed to sit overnight. A final heating at 75°C with frequent mixing is conducted until no signs of effervescence remain.

Once cooled, samples were centrifuged and rinsed repeatedly, and the sediment aliquots freeze-dried. Flash pyrolysis (CE-440 element analyzer, Exeter

Analytical Inc.) of 5 mg capsules yielded carbon concentrations (0.20% error) in the University of Alberta Biogeochemical Analytical Service Laboratory.

2.3.5. Microscopy

Charcoal content of sediments before and after the KMD digestion process was examined under light microscopy by settling slurries onto coverslips at room temperature. Once dry, these were mounted to slides using Naphrax. The pure inoculum was also imaged by scanning electron microscopy (SEM) using a JEOL field emission system at the University of Alberta.

2.4. Results

2.4.1. Spectroscopic analysis of charcoal dilution series

Spectroscopic absorbance patterns differ systematically across the VNIR spectral range in the charcoal-amended sediment series. Charcoal from the four individual tree species exhibit similar spectroscopic behavior across the measured wavelengths, implying that the charcoal standard faithfully represents the absorbance patterns of charcoal derived from mixed conifer species (Figure 2.4a). A general decrease in absorbance with increasing wavelength across the visible to near infrared portion of the spectrum is easily visible. Absorbance values range from 0.68 to 1.02 for the charcoal standard. Relative peaks in absorbance occur at approximately 550 nm and 1900 nm.

Similar to the charcoal standard, sediments from both lakes exhibit the highest absorbance values in the visible bands with declining absorbance extending into the near infrared portion of the spectrum (Figure 2.4b-c). Pure sediment matrices from both lakes demonstrate relative absorbance peaks at approximately 425 nm, 675 nm, 1400 nm, and 1900 nm. Whitebark Moraine Pond (Figure 2.4b) pure sediment absorbance values range from -0.069 to 0.40

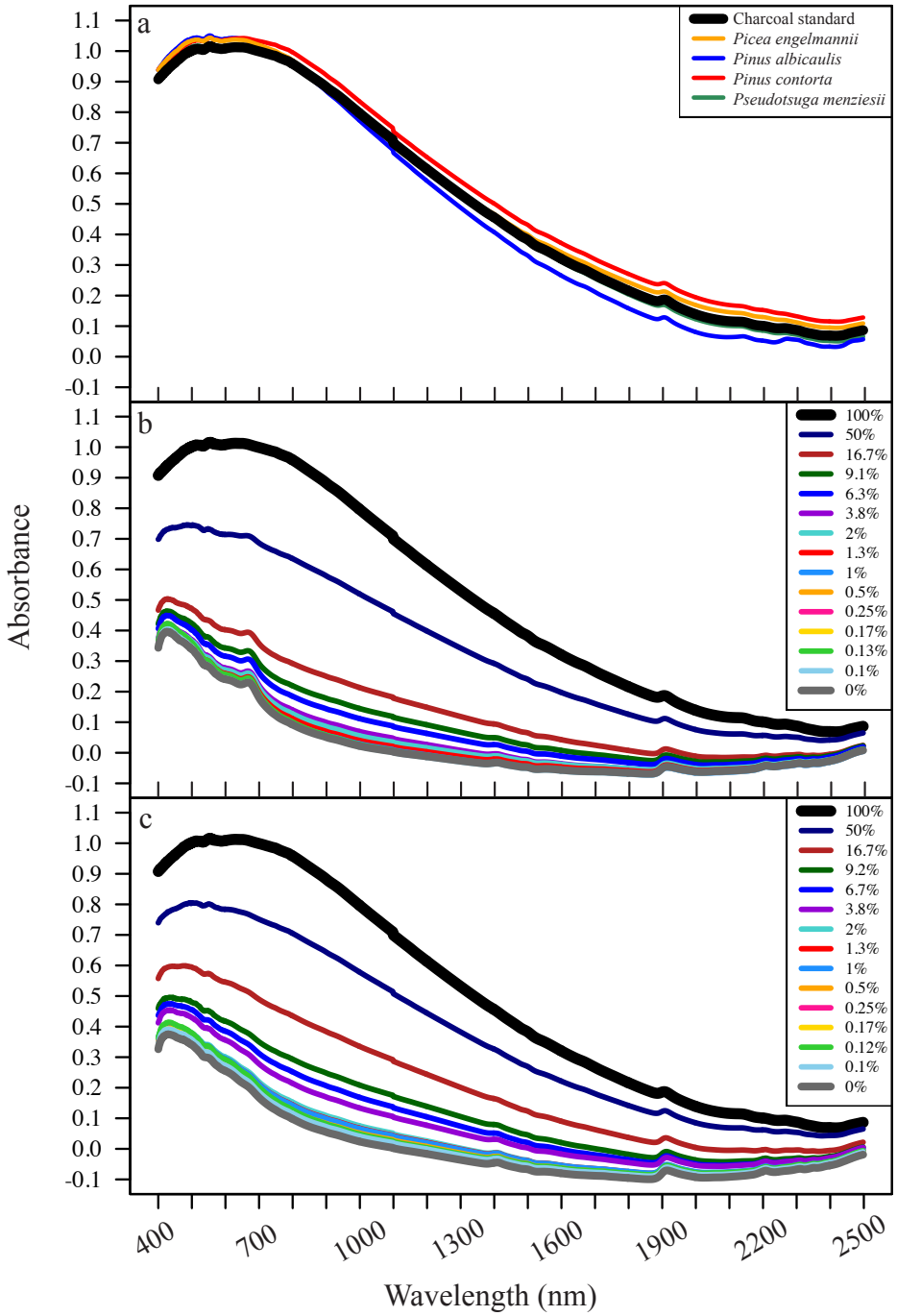

Figure 2.4. Charcoal calibration series. Charcoal standard established with equal mass mixture of the four tree species typical to forests in Grand Teton National Park (a). Sediment absorbance with included charcoal percentages by mass across the visible to near infrared spectrum for Whitebark Moraine Pond (b) and Ramshead Lake (c). The charcoal standard and pure sediment matrices are henceforth abbreviated 100% and 0% charcoal, respectively.

while Ramshead Lake (Figure 2.4c) expresses a slightly larger range from -0.99 to 0.37.

2.4.2. Statistical model calibration

Comparing the raw (unnormalized) and normalized absorbance patterns from the two lakes highlights the effects of statistical transformations to the spectra (Figure 2.5). Spectral normalization effectively removes negatives from both calibration datasets, stretching spectra and amplifying previously noted spectral features (Figure 2.5c-d). Spectroscopic differences between the lakes are intensified with normalization. Whitebark Moraine Pond exhibits a peak in relative absorbance within the red wavelengths (650 nm – 700 nm) while a slightly more prominent peak at 1900 nm is detectable in Ramshead Lake. Further data transformations for modeling purposes utilize both unnormalized and normalized datasets for each lake.

Area beneath the curve methods model absorbance variations at chlorophyll *a* and OH features (approximately 650 nm and 1900 nm, respectively). Linear regressions of area measurements beneath and between these features produce r^2 values of 0.93, 0.069, and 0.63 for Whitebark Moraine Pond and 0.98, 0.054, and 0.54 for Ramshead Lake using methods 2a-c, respectively (Table 2.3).

Models using NDVI and OSAVI values produce high r^2 values using both the normalized and unnormalized data from both sediment matrices (r^2 = 0.99 and 0.91, r^2 = 0.98 and 0.82 for Whitebark Moraine Pond and Ramshead Lake sediments, respectively; Table 2.3). As expected, r^2 values are identical for these models because their respective spectral index equations only vary by a constant of 0.16 (Table 2.2). Linear regressions of both unnormalized and normalized spectra treated with BAI generate higher r^2 values than NDVI and OSAVI with r^2

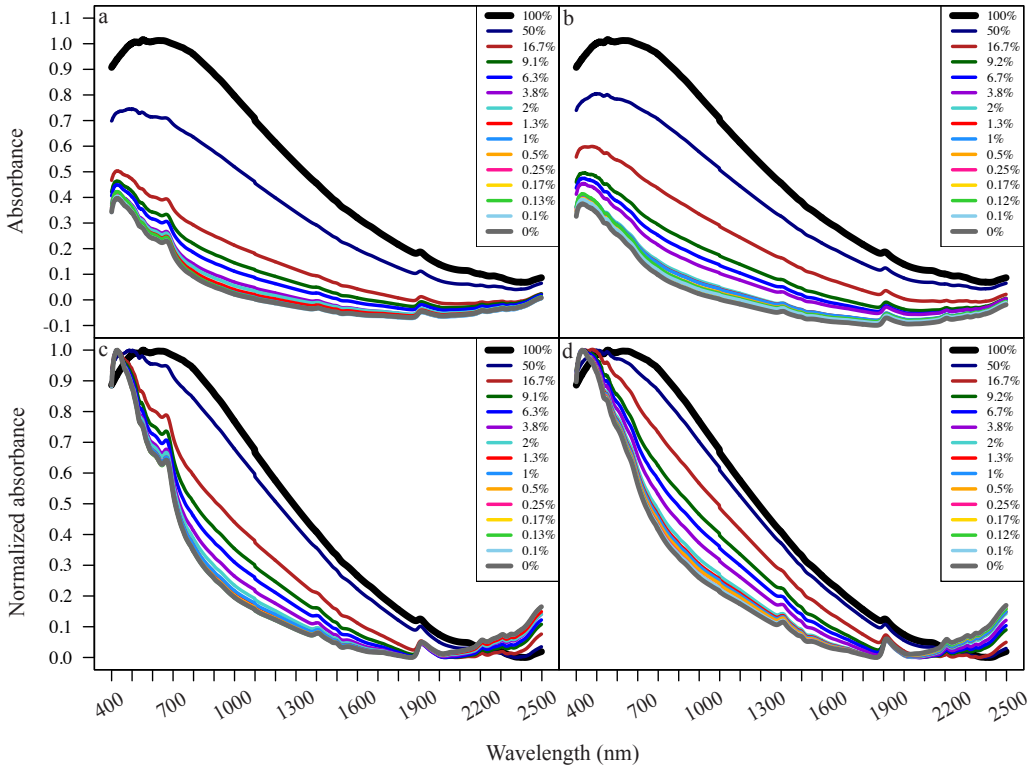

Figure 2.5. Calibration series comparison. Calibration datasets for Whitebark Moraine Pond (a, c) and Ramshead Lake (b,d). Plots (a) and (b) display the measured absorbance values while calibrations in plots (c) and (d) have been normalized. A stretching of spectral features is readily apparent in the normalized spectra.

Table 2.3. Modeling method results. Numbers correspond to methods attempted in Table 2.2. ABS abbreviates absolute value. R does not generate regression equations for PLSR so model equations are not included.

Lake	Method	Number	Data transformations		Model equation	r^2	RMSEP
			x	y			
Whitebark Moraine Pond	Area beneath curve	2a	log(1 + Charcoal %)	log(1 + Area)	y = 0.065x + 2.62	0.93	
		2b		log(Area)	y = -0.0016x + 2.49	0.069	
		2c		log(Area)	y = 7.14x + 267.89	0.63	
	NDVI	3a	log(1 + Charcoal %)		y = 0.55x - 0.29	0.91	
		3b	log(1 + Charcoal %)		y = 0.16x + 0.28	0.99	
	OSAVI	4a	log(1 + Charcoal %)		y = 0.55x - 0.13	0.91	
		4b	log(1 + Charcoal %)		y = 0.16x + 0.44	0.99	
	BAI	5a		log(BAI)	y = -0.019x + 5.09	0.99	
		5b			y = -0.029x + 4.63	0.99	
	Standard deviation	6	log(1 + Charcoal %)		y = -0.25x + 0.58	0.95	
	Slope	7			$y = -5.03e^{-6}x - 6.20e^{-5}$	0.98	
	PLSR	8a	1st derivative	1st derivative		0.92	7.28
		8a	2nd derivative	2nd derivative		0.87	9.56
		8b	1st derivative	1st derivative		0.97	4.29
		8b	2nd derivative	2nd derivative		0.90	8.32
		8c	1st derivative	1st derivative		0.97	4.92
		8c	2nd derivative	2nd derivative		0.90	8.33
		8d	1st derivative	1st derivative		0.93	7.13
		8d	2nd derivative	2nd derivative		0.88	9.32
Ramshead Lake	Area beneath curve	2a	log(1 + Charcoal %)	log(1 + Area)	y = 0.044x + 2.68	0.98	
		2b		log(Area)	y = -0.0019x + 2.47	0.054	
		2c		log(Area)	y = 6.32x + 359.77	0.54	
	NDVI	3a	log(1 + Charcoal %)		y = 0.41x = 0.041	0.82	
		3b	log(1 + Charcoal %)		y = 0.11x + 0.39	0.98	
	OSAVI	4a	log(1 + Charcoal %)		y = 0.41x - 0.12	0.82	
		4b	log(1 + Charcoal %)		y = 0.11x + 0.55	0.98	
	BAI	5a		log(BAI)	y = -0.023x + 5.09	0.99	
		5b		log(BAI)	y = -0.033x + 4.50	0.99	
	Standard deviation	6	log(1 + Charcoal %)		y = -0.22x + 0.48	0.99	
	Slope	7	log(1 + Charcoal %)	log(ABS(Slope))	y = 0.40x - 4.10	0.99	
	PLSR	8a	1st derivative	1st derivative		0.92	7.28
		8a	2nd derivative	2nd derivative		0.87	9.56
		8b	1st derivative	1st derivative		0.97	4.29
		8b	2nd derivative	2nd derivative		0.90	8.32
		8c	1st derivative	1st derivative		0.97	4.92
		8c	2nd derivative	2nd derivative		0.90	8.33
		8d	1st derivative	1st derivative		0.93	7.13
		8d	2nd derivative	2nd derivative		0.88	9.32

= 0.99 for Whitebark and Ramshead (Table 2.3).

The standard deviation model creates a new metric for analyzing spectral variance by comparing wavelengths with the highest and lowest absorbance values (452 nm and 860 nm, respectively; Table 2.2). Linear regressions of these values subsequently produce r^2 values of 0.95 in Whitebark and 0.99 in Ramshead datasets (Table 2.3).

The slope method ($Slope_{1500 - 1850\ nm}$) utilizes linear slope coefficients of near infrared spectra between the two areas of OH activity (1500 nm – 1850 nm) as indices for linear regression. Models based on this method generate r^2 values of 0.98 and 0.99 for Whitebark and Ramshead dilution series, respectively (Table 2.3).

PLSR performed on specific ranges of the visible to near infrared spectrum (as detailed in Table 2.2) were compared using r^2 and RMSEP (Table 2.3). RMSEP cannot be calculated for linear models, thus only PLSR regressions denote this field. All PLSR models using absorbance data transformed by the 1st derivative were calculated using three components; 2nd derivative datasets only required two components to reach optimum RMSEP values. Table 2.3 details the statistical results of the PLSR as well as all methods previously described.

The four highest statistically performing models, as determined by r^2 values approaching 1 and low RMSEP values, are the $NDVI_{normalized}$, $BAI_{unnormalized}$, $Slope_{1500 - 1850\ nm}$, and $PLSR_{800 - 2498\ nm}$ (1st derivative, 800 nm – 2498 nm) applied to the Whitebark Moraine Pond sediments (3b, 5a, 7, 8b, respectively; Table 2.2-3). These four models are explored further (Figure 2.6) by visually displaying the measured *versus* inferred charcoal percentages from each model regression. Because the first paleoenvironmental applications of this technique will be applied to Whitebark Moraine Pond in Chapter 3, further refinements to the models are restricted to this site. Refitted regressions were developed for the 0 – 10%

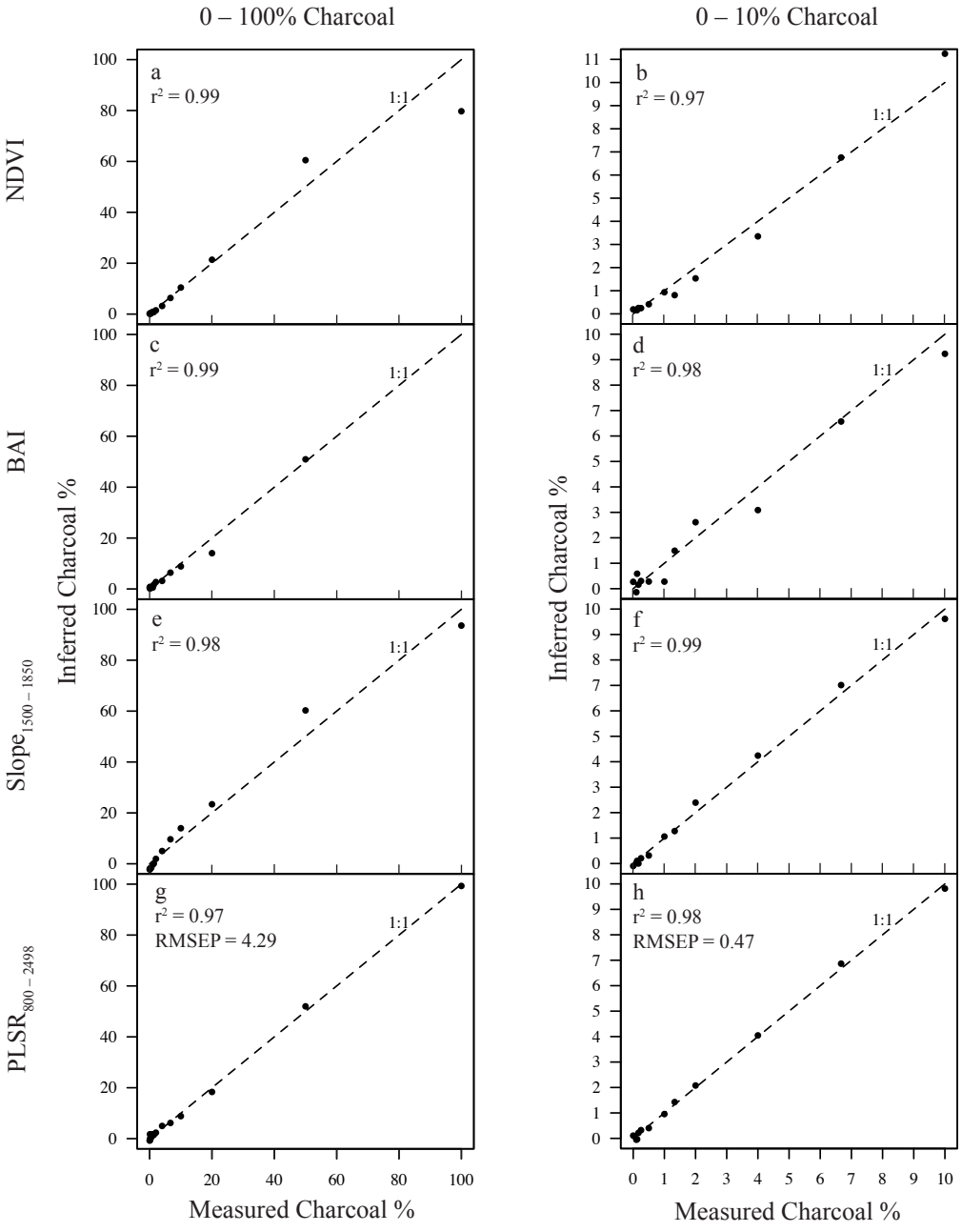

Figure 2.6. Highest statistically performing models. Models used and respective measured *versus* inferred charcoal include normalized NDVI (a, b), unnomalized BAI (c, d), $Slope_{1500-1850}$ (e, f), and 1st derivative $PLSR_{800-2498\ nm}$ (g, h). All models were reworked between 0 – 10% charcoal for (b, d, f, and g). All r^2 and RMSEP values represent error calculated from the models, not error calculated from the 1:1 line.

charcoal inoculum (instead of 0 – 100%) in order to zero in on the range of concentrations most likely to be expressed in Holocene sediments (Figure 2.6b, d, f, h).

All models, except the $Slope_{1500-1850\ nm}$ (7) and $PLSR_{800-2498\ nm}$ (8b) model, fail to improve statistically when refined below 10% charcoal (Table 2.4). Both the $Slope_{1500-1850\ nm}$ and PLSR models reveal slight increases of r^2 values (0.99 and 0.98, respectively) with the $PLSR_{800-2498\ nm}$ model also decreasing RMSEP dramatically from 4.29 to 0.47. The refined $PLSR_{800-2498\ nm}$ model only requires two components to attain this low RMSEP, as compared to three components when including the entire dilution series.

2.4.3. Conversion to % black carbon

Black carbon quantified (as % C) using KMD digestion of sediments incrementally spiked with known charcoal concentrations (% charcoal) generate a linear regression of $y = 0.5\ x + 3.1$ ($r^2 = 0.99$; Figure 2.7a). Refining the model to only include 0 – 10% charcoal adjusts the linear model to $y = 0.6\ x + 2.8$ ($r^2 = 0.86$; Figure 2.7b). Inferred KMD % C plots closely along a 1:1 line when compared to measured KMD % C for both the 0 – 100% and 0 – 10% charcoal models, confirming the fit and predictive power of the models (Figure 2.7c).

However, Figure 2.7d demonstrates that inferred % C values calculated from the 0 – 10% charcoal model plot closer to the 1:1 line, especially within 2.5 to 3.5% KMD measured black carbon. Despite a lower r^2 value of 0.86, the 0 – 10% charcoal model has a considerably smaller sum of residuals (-0.000073) as compared to the 0 – 100% charcoal model (-0.21; $r^2 = 0.99$) throughout the lower KMD % C ranges, which are of primary concern for this project (Table 2.5). We thus conclude that this is the best model for paleoenvironmental reconstruction using spectrally inferred charcoal concentrations from Whitebark Moraine Pond

Table 2.4. Refined model (0 – 10% charcoal) statistical performance comparisons.

Method	Number	Data Transformations		Model Equation	r^2	RMSEP
		x	y			
NDVI	3b	log(1 + Charcoal %)		y = 0.16x + 0.28	0.97	
BAI	5a		log(BAI)	y = -0.017x + 5.08	0.98	
$Slope_{1500-1850\ nm}$	7			$y = -8.39e^{-6}x - 5.16e^{-5}$	0.99	
$PLSR_{800-2498\ nm}$	8b	1st derivative	1st derivative		0.98	0.47

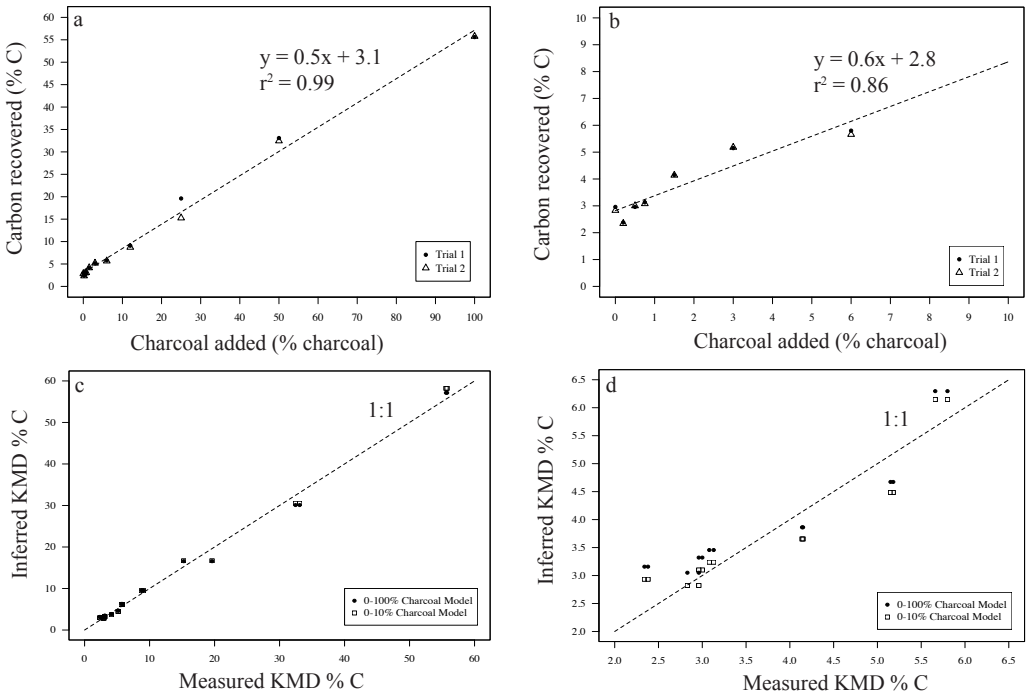

Figure 2.7. KMD model comparison. KMD calibration models between 0 – 100% charcoal and refined to 0 – 10% charcoal (a, b, respectively). Measured *versus* inferred KMD % C from both calibration models for 0 – 100% charcoal and 0 – 10% charcoal (c, d, respectively).

Table 2.5. KMD model statistical comparison.

Model charcoal range	r^2	Sum of residuals (0 – 100% charcoal)	Sum of residuals (0 – 10% charcoal)
0 - 100%	0.99	0.00018	-0.21
0 - 10%	0.86	-2.88	-0.000073

sediments.

2.5. Discussion

2.5.1. Lake sediment analysis and applicability of charcoal calibrations

The amendments to both lake sediment matrices confirms that charcoal induces profound spectroscopic variations that differ from those associated with sediment organic matter, photosynthate content, and lithology. Whitebark Moraine Pond sediments, which are highly organic, exhibit a pronounced relative absorbance peak within the chlorophyll *a* band (650 nm – 700 nm) that is not readily apparent in the more minerogenic Ramshead Lake sediments (Michelutti *et al.*, 2005, 2010; Wolfe *et al.*, 2006). Conversely, Ramshead Lake sediments express larger OH absorbance features at both 1400 nm and 1900 nm. This spectroscopic exploration of sediment matrices supports the general concept of ultimately creating a single, comprehensive spectroscopic charcoal calibration applicable to multiple study sites. However, at this point in time, the fundamental spectroscopic differences observed limit the calibration to the individual lakes from which they were derived.

2.5.2. Calibration analysis and superior model determination

The charcoal dilution series of both Whitebark Moraine Pond and Ramshead Lake effectively demonstrate that lake sediment absorbance values increase with higher charcoal concentrations across the VNIR spectrum. Unfortunately, for quantification purposes, we cannot attribute specific absorbance peaks or spectral activity in certain wavelengths directly to the presence of charcoal within a sediment matrix. This reality reflects the spectroscopically amorphous character of conifer charcoal. However, the overall effect of pyrogenic carbon opacity amplifies absorbance incrementally with charcoal

concentration, affording multiple opportunities to model the indirect effects of charcoal on VNIR spectra as a whole, ultimately allowing calibration and quantification.

The charcoal dilution series proves quite conducive to calibration efforts. Table 2.3 protests to the multitude of statistical approaches that readily describe some or most of the variance in the spectral dataset. It is important to note the particularly high r^2 values attainable for the various methods utilized. However, the reasoning behind targeting certain bands within the VNIR spectrum proves just as important as the significance levels of results.

Calibration models capture the effect charcoal transmits onto pre-existing spectral features reflecting organic and mineral properties. Area beneath the curve models attempt to measure the dampening of chlorophyll *a* and OH features with increased charcoal concentrations. However, determining a predictive model based on two independently varying components (e.g. charcoal concentration and lake primary productivity) inherently imparts elements of uncertainty into subsequent environmental reconstructions. Because NDVI, OSAVI, and BAI were developed for vegetation and post-fire landscape analysis, each rely heavily upon the red portion of the spectrum, wherein paleoecological studies focus upon this realm for estimations of previous biologic activity (Chuvieco *et al.*, 2002; Michelutti *et al.*, 2005, 2010; Wolfe *et al.*, 2006; Smith *et al.*, 2010). Consequently, we also lose confidence in predictions based on spectral indices for their potential to combine entities of separate biologic responses, despite their favorable statistical performances within the 0 – 100% and 0 – 10% charcoal ranges.

However, summarizing the complex relationship of absorbance spectra to various environmentally driven biologic and chemical responses using the proposed standard deviation method goes too far in the opposite

direction. Relying simply upon the difference in absorbance measurements from wavelengths maximizing variance in the pure sediment sample potentially leaves out a large array of data and hence information relating to the charcoal concentration of sediments.

Further, when deciding between models based on normalized *versus* unnormalized data, we determine that unnormalized data more closely represent the spectroscopic behavior of the investigated sediments. Figure 2.5 visually demonstrates the modifications normalization imparts upon the affected spectra. Data normalization holds the potential to affect spectral charcoal determination, inadvertently adjusting paleofire reconstructions. Thus, models based on the unnormalized spectra not only prove to be the most parsimonious, but also the best statistically and theoretically performing models.

Deciding on the most accurate model among the PLSR experiments relies on the comparison of calculated RMSEP values. Because RMSEP states the prediction error in the same units of measure (i.e. % charcoal), the PLSR models ultimately reveal relatively high error margins. Most models generate charcoal estimates with >5% error (Table 2.3), which is high considering the optimum scale we estimate lake charcoal inclusions (<10%).

$Slope_{1500 - 1850\ nm}$ and $PLSR_{800 - 2498\ nm}$ emerge as the highest statistically and theoretically performing models. Additionally, both models improve statistically when refined below 10% charcoal with r^2 values exceeding 0.98 for both approaches and RMSEP below 0.50 for the $PLSR_{800 - 2498\ nm}$ model (Table 2.5). Determination of the highest performing calibration ultimately hinges upon real-world applicability, which is explored further in Chapter 3. For now, we can confirm that the $Slope_{1500 - 1850\ nm}$ model produces the most realistic charcoal reconstructions and best matches KMD % C measurements from Whitebark Moraine Pond sediment cores. Thus, we put forth the proposed $Slope_{1500 - 1850}$

$_{nm}$ model to most accurately predict included charcoal concentration from spectroscopically measured sediment matrices.

2.5.3. KMD % carbon calibration analysis

Despite a lower r^2 value, the 0 – 10% charcoal model best represents included KMD % C (Figure 2.7; Table 2.5). Figure 2.7d visually demonstrates the increased accuracy of predictions from the 0 – 10% charcoal model at low KMD % C concentrations, particularly within 2.5 to 3.5 measured KMD % C. Additionally, a significantly smaller sum of residuals (-0.000073 as compared to -0.21 for 0 – 100% charcoal model) attests to the predictive skill of the 0 – 10% charcoal model.

Considering our focus on the applicability to natural examples, a refined KMD % C calibration appears most fitting. Basing a calibration model on samples ultimately unfeasible in real-world scenarios (e.g. 100% charcoal) gives undue bearing and statistical weight to unrealistic circumstances. Thus, refining the KMD % C calibration models below 10% included charcoal better estimates lower charcoal conditions and effectively grounds predictions.

Of note is the carbon content of our charcoal standard. Based on pyrolysis, the pure charcoal standard collected in the field and subsequently used to inoculate all sediment samples contains only 55.69% C after complete digestion of all other organic matter. The carbon concentration of our charcoal standard is less than expected, probably a result of the intense digestion process destroying less combusted phases of charcoal. This observation brings to light the range of C content possible within the spectrum of black carbon owing to the type of biomass burned and combustion conditions (Hedges *et al.*, 2000; Masiello, 2004; Haberstroh *et al.*, 2006), opening Pandora's box on potential carbon and charcoal estimation errors when reconstructing paleofire events. A full investigation into

the relationship of burn conditions to charcoal absorbance patterns is beyond the scope of this study.

However, we suggest this potential error source lies exclusively within the KMD % C conversion step of our methodology, not affecting spectroscopic charcoal detection. The four conifer species with unknown, but probably similar, burn conditions produce spectrally similar absorbance patterns, all of which are approximated within the 1:1:1:1 charcoal standard mixture (Figure 2.4a). Additionally, the calibration models utilize general opacity imparted upon sediments by the charcoal standard as reference for charcoal content, which, by our spectroscopic measurements, is not excessively affected by differing burn conditions in the VNIR spectrum. Thus, the charcoal concentrations are not adversely affected by unknown burn conditions.

The conversion of charcoal content to KMD % C to verify down-core carbon content consequently contains higher potential for absolute error. However, this comes with the territory of black carbon analyses, each with their own operational definition of the term "black carbon" (Haberstroh *et al.*, 2005; Conedera *et al.*, 2009). We aim to mitigate these problems by decomposing peaks in reconstructed KMD % C data through time-series analysis in Chapter 3 to approximate millennial-scale trends in fire occurrence across the Holocene with no intention to reconstruct relative burn conditions from the paleorecord.

2.6. Conclusion

Calibration of lake sediments amended with a charcoal standard demonstrates the feasibility of spectroscopic charcoal quantification for highly-resolved paleofire records. Development and analysis of various spectral indices, statistical treatments, and data transformations for data summarization reveal a number of statistically significant and hence viable models for data

transformation. The model developed from linear slope coefficients between 1500 nm to 1850 nm emerges as the most skilled model within the 0 – 10% charcoal range, with the potential to produce the most realistic down-core charcoal reconstructions from Whitebark Moraine Pond sediments. Validation of spectrally-inferred charcoal concentrations is now possible with the successful calibration of KMD % C to the Whitebark Moraine Pond sediment charcoal dilution series. The VNIR spectroscopic charcoal quantification methodology proposed in this chapter offers a rapid, non-destructive alternative to optical microscopy for paleofire determination and fire history reconstruction from lake sediment matrices.

2.7. References

Bellon-Maurel, V. & McBratney, A. 2011. Near-infrared (NIR) and mid-infrared (MIR) spectroscopic techniques for assessing the amount of carbon stock in soils – Critical review and research perspectives. Soil Biology & Biochemistry 43: 1398-1410.

Bowman, D.M.J.S., Balch, J.K., Artaxo, P., Bond, W.J., Carlson, J.M., Cochrane, M.A., D'Antonio, C.M., DeFries, R.S., Doyle, J.C., Harrison, S.P., Johnston, F.H., Keeley, J.E., Krawchuk, M.A., Kull, C.A., Marston, J.B., Moritz, M.A, Prentice, I.C., Roos, C.I., Scott, A.C., Swetnam, T.W., van der Werf, G.R., Pyne, S.J. 2009. Fire in the Earth system. Science 324: 481-484.

Brunelle, A., Whitlock, C., Bartlein, P., Kipfmueller, K. 2005. Holocene fire and vegetation along environmental gradients in the Northern Rocky Mountains. Quaternary Science Reviews 24: 2281-2300.

Carcaillet, C., Bouvier, M., Fréchette, B., Larouche, A.C., Richard, P.J.H. 2001. Comparison of pollen-slide and sieving methods in lacustrine charcoal analyses for local and regional fire history. The Holocene 11: 467-476.

Chuvieco, E., Martin, M.P., Palacios, A. 2002. Assessment of different spectral indicies in the red-near-infrared spectral domain for burned land discrimination. International Journal of Remote Sensing 23: 5103-5110.

Conedera, M., Tinner, W., Neff, C., Meurer, M., Dickens, A.F., Krebs, P. 2009. Reconstructing past fire regimes: methods, applications, and relvance to fire management and conservation. Quaternary Science Reviews 28: 555-576.

Cozzolino, D. & Morón, A. 2006. Potential of near-infrared reflectance spectroscopy and chemometrics to predict soil organic carbon fractions. Soil & Tillage Research 85: 78-85.

Enache, M.D. & Cumming, B.F. 2006. Tracking recorded fires using charcoal morphology from the sedimentary sequence of Prosser Lake, British Columbia (Canada). Quaternary Research 65: 282-292.

Flannigan, M.D., Krawchuk, M.A., de Groot, W.J., Wotton, B.M., Gowman, L.M. 2009. Implications of changing climate for global wildland fire. International Journal of Wildland Fire 18: 483-507.

Glew, J.R. 1991. Miniature gravity corer for recovering short sediment cores. Journal of Paleolimnology 5: 285-287.

Haberstroh, P.R., Brandes, J.A., Gélinas, Y., Dickens, A.F., Wirick, S., Cody, G. 2006. Chemical composition of the graphitic black carbon fraction in riverine and marine sediments at sub-micron scales using carbon X-ray spectromicroscopy. Geochimica et Cosmochimica Acta 70: 1483-1494.

Hedges, J.I., Eglinton, G., Hatcher, P.G., Kirchman, D.L., Arnosti, C., Derenne, S., Evershed, R.P., Kögel-Knabner, I., de Leeuw, J.W., Littke, R., Michaelis, W., Rullkötter, J. 2000. The molecularly-uncharacterized component of nonliving organic matter in natural environments. Organic Geochemistry 31: 945-958.

Higuera, P.E., Whitlock, C., Gage, J.A. 2010. Linking tree-ring and sediment-charcoal records to reconstruct fire occurrence and area burned in subalpine forests of Yellowstone National Park, USA. The Holocene 21: 327-341.

Huerta, M.A., Whitlock, C., Yale, J. 2009. Holocene vegetation-fire-climate linkages in northern Yellowstone National Park, USA. Palaeogeography, Palaeoclimatology, Palaeoecology 271: 170-181.

Jacobs, K. & Whitlock, C. 2008. A 2000-year environmental history of Jackson Hole, Wyoming, inferred from lake-sediment records. Western North American Naturalist 68: 350-364.

Kurth, V.J., MacKenzie, M.D., DeLuca, T.H. 2006. Estimating charcoal content in forest mineral soils. Geoderma 137: 135-139.

Laird, L.D. & Campbell, I.D. 2000. High resolution palaeofire signals from Christina Lake, Alberta: a comparison of the charcoal signals extracted by two different methods. Palaeogeography, Palaeoclimatology, Palaeoecology 164: 111-123.

Malley, D.F. 1998. Near-infrared spectroscopy as a potential method for routine sediment analysis to improve rapidity and efficiency. Water Science and Technology 37: 181-188.

Malley, D., Lockhart, L., Wilkinson, P., Hauser, B. 2000. Determination of carbon, carbonate, nitrogen, and phosphorous in freshwater sediments by near-infrared reflectance spectroscopy: rapid analysis and a check on conventional analytical methods. Journal of Paleolimnology 24: 415-425.

Malley, D., Williams, P.C., Stainton, M. 1996. Rapid measurement of suspended C, N, and P from Precambrian shield lakes using near-infrared reflectance spectroscopy. Water Research 30: 1325-1332.

Marlon, J.R., Bartlein, P.J., Gavin, D.G., Long, C.J., Anderson, R.S., Briles, C.E., Brown, K.J., Colombaroli, D., Hallett, D.J., Power, M.J., Scharf, E.A., Walsh, M.K. 2012. Long-term perspective on wildfires in the western USA. PNAS: E535-E543

Marlon, J.R., Cui, Q., Gaillard, M.-J., McWethy, D., Walsh, M. 2010. Humans and fire: Consequences of anthropogenic burning during the past 2 ka. PAGES news 18: 80-82.

Masiello, C.A. 2004. New directions in black carbon organic geochemistry. Marine Chemistry 92: 201-213.

Menges, F. 2011. Spekwin32 - optical spectroscopy software. Version 1.71.6. URL: http://www.effemm2.de/spekwin/.

Mevik, B-H. & Wehrens, R. 2007. The pls package: principle component and partial least squares regression in R. Journal of Statistical Software 18: 1-24.

Michelutti, N., Blais, J.M., Cumming, B.F., Paterson, A.M., Rühland, K., Wolfe, A.P., Smol, J.P. 2010. Do spectrally inferred determinations of chlorophyll a reflect trends in lake trophic status? Journal of Paleolimnology 43: 205-217.

Michelutti, N., Wolfe, A.P., Vinebrooke, R.D., Rivard, B., Briner, J.P. 2005. Recent primary production increases in arctic lakes. Geophysical Research Letters 32: L19715, doi:10.1029/2005GL023693.

Millspaugh, S.H. & Whitlock, C. 1995. A 750-year fire history based on lake sediment records in central Yellowstone National Park. USA. The Holocene 5: 283-292.

Millspaugh, S.H., Whitlock, C., Bartlein, P.J. 2000. Variations in fire frequency and climate over the past 17 000 yr in central Yellowstone National Park. Geology 28: 211-214.

Mooney, S.D. & Tinner, W. 2011. The analysis of charcoal in peat and organic sediments. Mires and Peat 7: 1-18.

R Development Core Team. 2011. R: A language and environment for statistical computing. R Foundation for Statistical Computing, Vienna, Austria. ISBN 3-900051-07-0. URL: http://www.R-project.org/.

Romme, W.H. & Despain, D.G. 1989. Historical perspective on the Yellowstone fires of 1988. BioScience 39: 695-699.

Romme, W.H., Boyce, M.S., Gresswell, R., Merril, E.H., Minshall, W., Whitlock, C., Turner, M.G. 2011. Twenty years after the 1988 Yellowstone fires: lessons about disturbance and ecosystems. Ecosystems DOI: 10.1007/s10021-011-9470-6

Rosén, P., Dåbakk, E., Renberg, I., Nilsson, M., Hall, R. 2000. Near-infrared spectrometry (NIRS): a new tool for inferring past climatic changes from lake sediments. The Holocene 10: 161-166.

Rosén, P. & Hammarlund, D. 2007. Effects of climate, fire and vegetation development on Holocene changes in total organic carbon concentration in three boreal forest lakes in northern Sweden. Biogeosciences 4: 975-984.s

Schoennagel, T., Veblen, T.T., Romme, W.H. 2004. The interaction of fire, fuels, and climate across Rocky Mountain forests. BioScience 54: 661-676.

Smith, A.M.S., Eitel, J.U.H., Hudak, A.T. 2010. Spectral analysis of charcoal on soils: implications for wildland fire severity mapping methods. International Journal of Wildland Fire 19: 976-983.

Westerling, A.L., Turner, M.G., Smithwick, E., Romme, W.H., Ryan, M.G. 2011. Continued warming could transform greater Yellowstone fire regimes by mid-21st century. Proceedings of the National Academy of Sciences of the United States of America 108: 13165-13170.

Whitlock, C. 1993. Postglacial vegetation and climate of Grand Tetons and Southern Yellowstone National Parks. Ecological Monographs 63: 173-198.

Whitlock, C., Dean, W.E., Fritz, S.C., Stevens, L.R., Stone, J.R., Power, M.J., Rosenbaum, J.R., Pierce, K.L., Bracht-Flyr, B.B. 2012. Holocene seasonal variability inferred from multiple proxy records from Crevice Lake, Yellowstone National Park, USA. Palaeogeography, Palaeoclimatology, Palaeoecology 331-332: 90-103.

Whitlock, C. & Larsen, C. 2001. Charcoal as a fire proxy. In Tracking Environmental Change Using Lake Sediments: Volume 3 Terrestrial, Algal, and Siliceous indicators; Smol, J.P., Birks, H.J.B., and Last. W.M. Kluwer Academic Publishers, Dordrecht: 75-97.

Whitlock, C., Marlon, J., Briles, C., Brunelle, A., Long, C., Bartlein, P. 2008. Long-term relations among fire, fuel, and climate in the north-western US based on lake-sediment studies. International Journal of Wildland Fire 17: 72-83.

Whitlock, C. & Millspaugh, S.H. 1996. Testing the assumptions of fire-history studies: An examination of modern charcoal accumulation in Yellowstone National Park, USA. Holocene 6: 7-16.

Wolfe, A.P., Vinebrooke R.D., Michelutti N., Rivard B., Das B. 2006. Experimental calibration of lake-sediment spectral reflectance to chlorophyll a concentrations: methodology and paleolimnological validation. Journal of Paleolimnology 36: 91-100.

CHAPTER 3

A SPECTROSCOPICALLY-INFERRED HOLOCENE FIRE HISTORY FROM GRAND TETON NATIONAL PARK, WYOMING

3.1. Introduction

Lake sediments offer the most temporally extensive record of fire−climate−vegetation relationships. Charcoal and pollen serve as direct proxies for fire occurrence and associated vegetation responses, effectively enabling inferences of paleoclimatic conditions. Traditional charcoal enumeration techniques lack methodological standardization, which hampers the interpretation of results and comparison between studies (Laird & Campbell, 2000; Carcaillet *et al.*, 2001; Whitlock & Larsen, 2001; Tinner & Hu, 2003; Conedera *et al.*, 2009). Additionally, time-consuming laboratory techniques allow various biases and inaccuracies to seep into optical charcoal datasets.

The spectroscopic method for charcoal quantification proposed in the previous chapter aims to mitigate many of the problems associated with conventional optical microscopy charcoal techniques. Spectroscopic measurements can be completed in a fraction of the time required for microscopic charcoal determinations, and thus can generate stratigraphically continuous fire records with reproducible results that are expressed in a metric readily comparable between various studies (i.e. % charcoal by mass).

Chapter 2 presented a multitude of statistically viable calibration techniques relating charcoal concentrations to lake sediment absorbance patterns, all of which rely upon the general opacity charcoal imparts upon sediment matrices within the visible to near-infrared (VNIR) spectrum. In this chapter,

we further investigate the top four statistically performing models ($NDVI_{normalized}$, $BAI_{unnormalized}$, $Slope_{1500 - 1850\ nm}$, and $PLSR_{800 - 2498\ nm}$) with down-core applications and comparison to measured black carbon concentrations. In combination with direct comparisons to historical fire occurrences, the down-core performance of the various models can be assessed rigorously.

The most effective calibration model was then applied to VNIR absorbance values from a composite chronology (Whitebark Moraine Pond, Grand Teton National Park, Wyoming) to reconstruct down-core charcoal concentrations. Utilizing the principles of paleofire analyses, wherein charcoal concentrations above a background charcoal component indicate discrete fire events (Whitlock & Millspaugh, 1996; Long *et al.*, 1998; Whitlock & Larsen, 2001), the spectrally-inferred charcoal time-series was subsequently decomposed to assess variability of Holocene fire frequency.

The Whitebark Moraine Pond paleofire reconstruction generated using environmental spectroscopy complements optically counted Holocene fire histories from Cygnet Lake (Yellowstone National Park, Wyoming) in the Greater Yellowstone Ecosystem (GYE). Thus, this contribution is not only methodological, but furthermore adds to the understanding of regional fire history reconstructions. The spectroscopic method produces temporally continuous paleofire reconstructions without sample destruction, requiring a fraction of the time and effort necessitated by conventional paleofire analyses. The increased practicality of generating and understanding long-term fire history information ultimately benefits fire managers, government officials, and the scientific community with practical application of the spectroscopic charcoal quantification methodology.

3.2. Site description

The remote Whitebark Moraine Pond (informal name, 43.79° N, 110.79° W; 2800 m asl; area: 0.76 ha; depth: 8 m) was chosen for regional paleofire assessment because its alpine lake records charcoal transported throughout the northern Rocky Mountain region (Figure 2.1). Whitebark Moraine Pond, formed by lateral and recessional Pinedale moraines damming the upper reaches of Paintbursh Canyon in Grand Teton National Park, owes its name and highly-organic (>20%) brown gyttia (sapropel) sediment content to the abundant Whitebark Pine (Pinus albicaulis) vegetating all but the western margin of the small catchment.

3.3. Methodology

3.3.1. Sediment core retrieval

Two cores were collected from Whitebark Moraine Pond in July 2010. A short (19.5 cm) core was retrieved using a modified K-B gravity corer (Glew, 1991), sectioned in the field in continuous 0.5 cm increments, and returned to the laboratory for freeze-drying and homogenization. All sample depths reflect the midpoint value of the sampled interval. A light percussion corer (Aquatic Research Inc. hammer core; http://www.aquaticresearch.com) was utilized to retrieve a longer (154.5 cm) core. The percussion core was kept whole and subsequently split in the lab with one half subsampled at 0.5 cm intervals before freeze-drying and homogenization. The remaining half of the core is archived at the University of Colorado, Boulder for future analyses.

3.3.2. Core chronology

Seventeen bulk sediment samples (2.5 g dry weight) from the gravity core were analyzed for ^{210}Pb activity by MyCore Scientific (Deep River, Ontario)

Table 3.1. Radiocarbon results (percussion core).

Absolute depth (cm)	Composite depth (cm)	Material	Age (^{14}C yr BP)	Age (cal yr BP)	
				2σ low	2σ high
17.75	25.75	conifer twig	555 ± 15	689	588
27.75	35.75	conifer bark	1185 ± 15	1232	1121
100.25	108.25	twig	4675 ± 20	5530	5381
120.75	128.75	twig	5685 ± 20	6560	6468
148.25	156.25	Mazama ash		7687 ± 150	
152.25	160.25	conifer cone	6960 ± 20	7907	7768

Table 3.2. ^{210}Pb results (gravity core).

Midpoint depth (cm)	^{210}Pb (Bq/g)	Age at top of section (year)	Standard deviation in date (years)
0.25	2.901	2010.6	0
0.5	2.298	2009.7	0
1.25	2.166	2008.3	0
1.75	1.909	2005.3	0
2.25	1.934	2002.1	1
2.75	1.651	1997.8	1
3.25	1.241	1994	1
3.75	1.127	1990	1
4.25	1.020	1986	2
4.75	0.951	1983	2
5.25	0.862	1978	2
6.25	0.561	1971	4
8.25	0.401	1961	11
12.25	0.478	1943	12
14.25	0.394	1928	23
16.25	0.346	1913	39
20.25	0.300	1873	120

and five accelerator mass spectrometry (AMS) ^{14}C dates were obtained on conifer macrofossils from the percussion core (Table 3.1-2). The ^{14}C targets were prepared at the Laboratory for AMS Radiocarbon Preparation and Research (Institute of Arctic and Alpine Research, University of Colorado, Boulder), whereas AMS measurements were conducted at the W.M. Keck Laboratory (University of California, Irvine). Radiocarbon results were calibrated using OxCal (version 4.1) based on the IntCal09 curve (Ramsey, 2001; Reimer *et al.*, 2009).

Additionally, Mazama tephra (7687 ± 150 BP, Zdanowicz *et al.*, 1999) was encountered 8.5 cm from the base of the percussion core. Geochemical analyses of individual vesiculate ash shards by electron microprobe analysis (JEOL-8900, University of Alberta) verify the identity of the tephra. A composite sedimentary record was derived by splicing together the two cores using CLAM (Blaauw, 2010) and the ^{210}Pb, ^{14}C, and tephra age constraints. All ages are reported as calendar years before present (cal yr BP), indicating their age relative to core collection in 2010. The resulting age model was applied to the spectroscopic results in developing the Holocene fire history, yielding a continuous composite record spanning nearly 8000 years.

3.3.3. Spectroscopic measurement

Spectroscopic measurements were made using a Model 6500 Rapid Content Analyzer (FOSS NIRSystems Inc.) on lyophilized and homogenized (<125 μm) samples of approximately 4 g each. Absorbance measurements (A=log(1/reflectance)) were taken at 2 nm intervals across visible to near-infrared wavelengths (400 nm – 2498 nm). Absorbance values of each sample represent an average of 32 scans. To compensate for spectral drift during the measurement process, measurements of the ceramic reference panel were made every four

samples and corrected for. Including reference panel adjustments, analysis time per sample was approximately one minute.

3.3.4. Statistical treatment

As detailed in Chapter 2, many data summation techniques were employed to relate variations in absorbance to charcoal concentrations (Table 2.2). The most statistically robust models ($NDVI_{normalized}$, $BAI_{unnormalized}$, $Slope_{1500 - 1850\ nm}$, and $PLSR_{800 - 2498\ nm}$ (1^{st} derivative)) were refined and refit below the 10% charcoal level (instead of 0 − 100%) with varying degrees of improvement in statistical power. These four refined models were first applied to absorbance values obtained from Whitebark Moraine Pond's most recent sediments (0 to 150 cal yr BP) to assess the best performance in a real-world scenario. Inferred % charcoal values were then converted to black carbon (Kurth, MacKenzie & DeLuca (KMD) % C) using the % charcoal to KMD % C conversion model for comparison to measured carbon levels from flash pyrolysis. Once the optimum model was selected, absorbance values from the composite chronology were run through the resultant model and KMD conversion to generate a continuous Holocene black carbon reconstruction.

3.3.5. Black carbon measurement

We adapted the Kurth *et al.* (2006) black carbon separation technique to analyze carbon content of the sediment core samples. Intervals chosen for analysis reflect both peaks and troughs in the reconstructed charcoal record, as determined by the $Slope_{1500 - 1850\ nm}$ model. Following the protocol we established in Chapter 2, 0.5 g of freeze-dried sediment sample was mixed with 20 mL of 30% H_2O_2 in a 250 mL Erlenmeyer flask and allowed to sit for 4 hours with constant mixing. Before digesting 19 hours, 10 mL of 1 M HNO_3 was added to

the mixture. Samples were heated to 50°C for 4 hours, occasionally mixed, and allowed to sit overnight. Constant mixing ensured samples did not boil over as they were heated at 75°C until they no longer showed signs of effervescence.

After cooling to room temperature, samples were centrifuged and rinsed repeatedly before freeze-drying. Flash pyrolysis (CE-440 element analyzer, Exeter Analytical Inc.; University of Alberta Biogeochemical Analytical Service Laboratory) of 5 mg capsules yielded sediment carbon concentrations (0.20% error). Reproducibility is approximately ± 0.2% C. Measuring carbon content of our charcoal standard before KMD analysis assessed carbon recovery rate. Utilizing the sediment charcoal content to black carbon conversion model from Chapter 2, we were able to reconstruct the down-core sediment carbon concentrations.

3.3.6. Decomposition of reconstructed charcoal time series

Inferred KMD % C concentrations were detrended using a cubic polynomial spline as described by Cook & Peters (1981) for the statistical decomposition of reconstructed black carbon concentrations and peak analysis. In this method, we resampled KMD % C values at pseudo-annual intervals and normalized interpolated values before using cubic splines with periods of 250 and 3000 years to highlight high- and low- frequency departures, respectively (Torrence & Compo, 1998). For peak analysis, both spline models were subtracted from normalized KMD % C values to detect positive anomalies, thus black carbon peaks, indicating fire events. Millennial fire frequency was calculated by counting exceedances from the 3000 year spline model. Wavelet analysis of both spline models measured variance in KMD % C results as well as periodicity of fire events.

3.4. Results

3.4.1. Core chronology

Radiocarbon-dated macrofossils from five intervals and the Mazama tephra provide a robust chronology on the percussion core, with no age reversals (Table 3.1). Ages (cal yr BP) were calibrated to 2σ for 95% confidence in the date results. The short core was dated for ^{210}Pb every half centimeter for the top 5 cm and intermittently thereafter (Table 3.2). Ages from the CLAM-derived spline model were plotted against core depth to reconstruct an age *versus* depth curve (Figure 3.1). The cores were spliced together so that 8.25 cm in the gravity core equals 0 cm in the percussion core. Using the CLAM age model, the base of the composite chronology (162.25 cm) was deposited 7931 cal yr BP. The tephra layer at 156.25 cm is attributed with confidence to the Mazama ash, originating from Mount Mazama (Oregon, USA) and dated 7687 ± 150 cal yr BP from layer counting its occurrence in Greenland ice (Figure 3.2; Zdanowicz *et al.*, 1999).

3.4.2. Spectroscopic measurements

The sediment core samples express similar absorbance patterns to the Whitebark Moraine Pond sediment standard (0% charcoal) utilized in the calibration series (Figure 3.3a). The highest absorbance values are noted in the visible wavelengths, decreasing into the near-infrared band. Relative peaks in absorbance occur within the red band (650 nm – 700 nm) and 1900 nm OH feature, along with variability at the 1400 nm OH feature, which are not constant between different sample depths (Figure 3.3b,e). A relatively uniform drop in absorbance values is noted across the entire VNIR spectrum with increased core depth (Figure 3.3a).

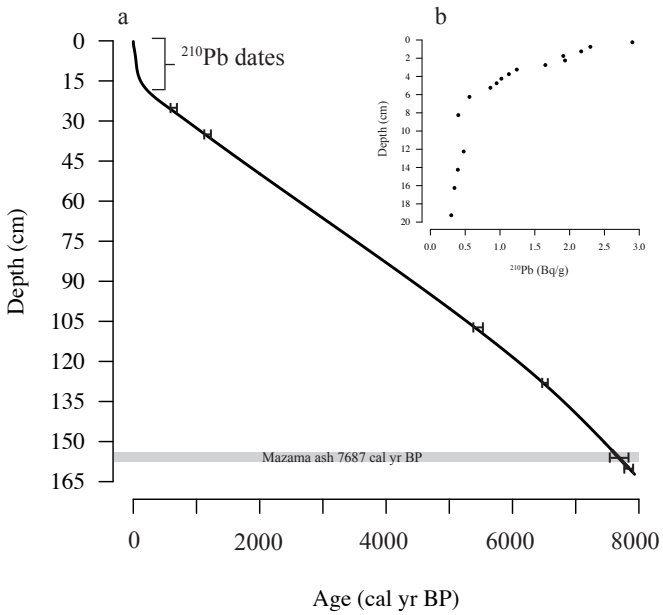

Figure 3.1. Whitebark Moraine Pond age *versus* depth plot. Age *versus* depth established by the CLAM age model (a). Error bars indicate 2σ estimates from the five calibrated radiocarbon dates. The top 19.5 cm are determined from ^{210}Pb measurements (b).

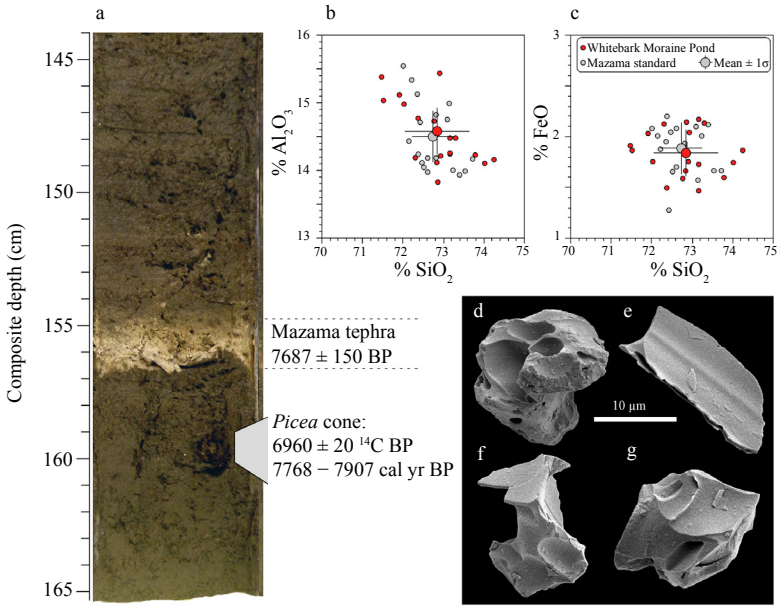

Figure 3.2 Tephra analysis. Stratigraphic image of tephra with composite depth and radiocarbon dated *Picea* cone (a). Geochemical analyis confirms similarity to Mazama tephra standard (b,c). SEM images of tephra samples from the Whitebark Moraine Pond percussion core (d-g).

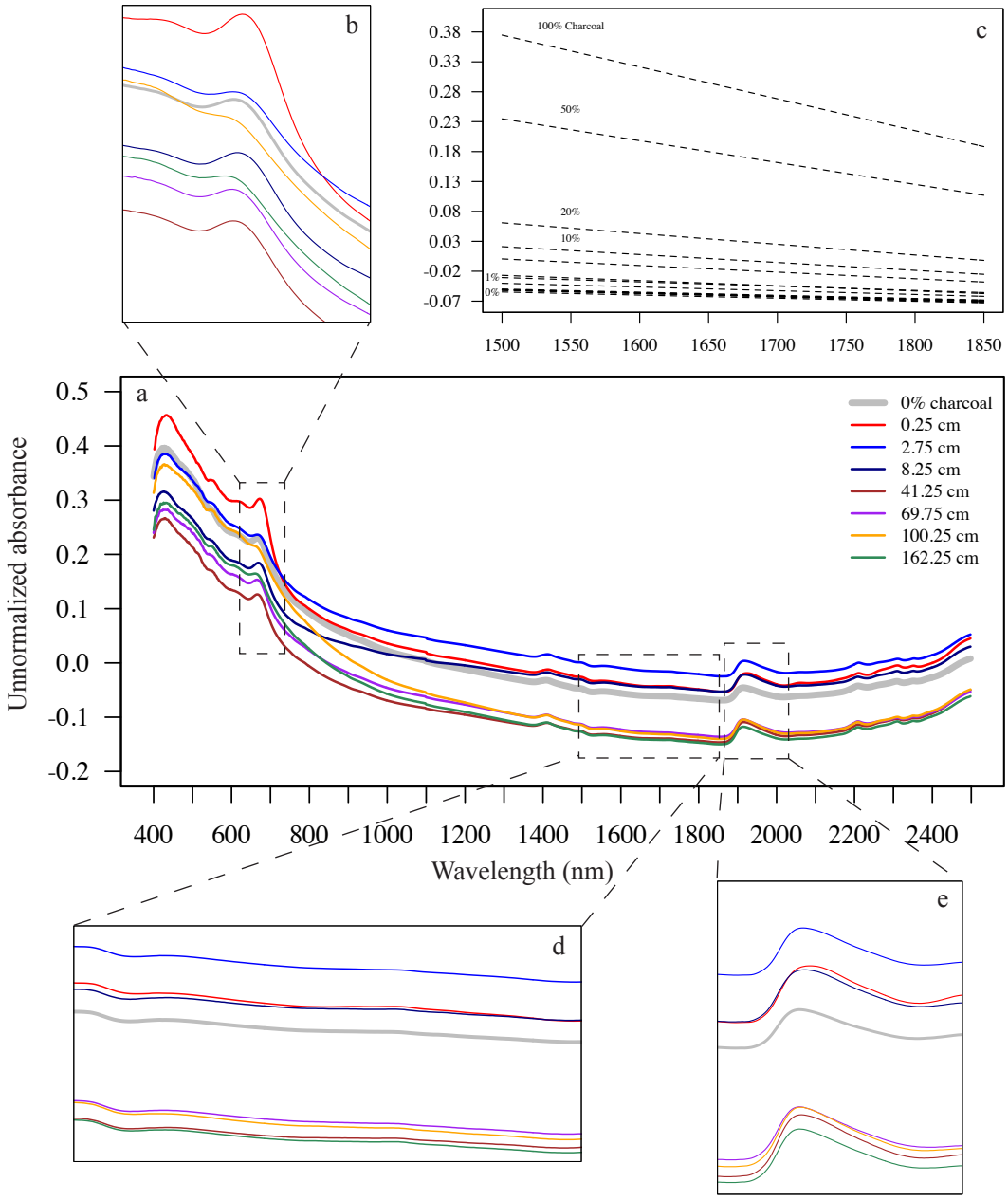

Figure 3.3. Whitebark Moraine Pond VNIR spectra. Absorbance measurements vary with increasing composite core depth (a). Spectral patterns differ within the Chlorophyll *a* band (b). Variation in the $Slope_{1500-1850\ nm}$ region (d) and OH band (e) lies only in overall absorbance drop, not in the shape of spectral features. Panel c) visually explains the incremental changes in slope within 1500 – 1850 nm with increasing charcoal concentration, which serves as the basis for the $Slope_{1500-1850\ nm}$ method.

3.4.3. KMD % C measurement and down-core charcoal model results

Duplicate measurements of KMD % C from the composite core vary throughout the investigated sample intervals (Table 3.3). Comparison of % C measurements from our charcoal standard before and after KMD analysis (Average % C: 56.67 and 55.66, respectively) reveals a carbon recovery rate of 98%. Black carbon measurements range from 1.44 to 2.82 % C with an apparent outlier of 3.92 % C at 98.25 cm. The range of KMD % C values measured from the composite core indicate charcoal levels lie below 0.5% included charcoal (2.96 – 3.00 % C), as compared to the KMD calibration results (Table 3.3).

Measured KMD % C values allow verification of spectrally-inferred charcoal concentrations. Reconstructing charcoal over the last 150 years using the four highest statistically performing models and converting results to KMD % C through the refined (0 – 10% charcoal) model ($y = 0.6\ x + 2.8$; $r^2 = 0.86$) reveals marked changes in inferred charcoal concentrations through time (Figure 3.4). All four models indicate that black carbon, and thus charcoal, levels have increased over the past 30 years after an unambiguous decrease around 40 cal yr BP. Both the $BAI_{unnormalized}$ and $PLSR_{800-2498\ nm}$ models reconstruct negative KMD % C, indicating biasing of reconstructed % charcoal levels prior to KMD conversion (Figure 3.4b,d).

To compute which charcoal model most closely reconstructs black carbon, the sum of residuals between the model results and measured KMD % C were calculated for each model. The sum of residuals (measurement of difference between data and estimation model results: $\Sigma(\%\ C_{measured} - \%\ C_{reconstructed})$) for each model are as follows: $NDVI_{normalized}$: 4.91, $BAI_{unnormalized}$: 19.62, $Slope_{1500-1850\ nm}$: 3.77, and $PLSR_{800-2498\ nm}$: 14.38. This calculation and visual analysis of black carbon results confirms the $Slope_{1500-1850\ nm}$ model most closely reproduces included black carbon concentrations, and thus charcoal, from the investigated

Table 3.3. Measured KMD % C values.

Sample	Composite depth (cm)	Measured % C	
		Trial 1	Trial 2
Charcoal standard (before KMD digestion)		56.70	56.64
Calibration series			
0% charcoal		2.96	2.83
0.2% charcoal		2.38	2.34
0.5% charcoal		2.96	3.00
0.75% charcoal		3.13	3.08
1.5% charcoal		4.15	4.14
3.0% charcoal		5.15	5.18
6% charcoal		5.80	5.66
12% charcoal		9.08	8.72
25% charcoal		19.61	15.26
50% charcoal		33.09	32.45
100% charcoal		55.61	55.77
Composite core	0.75	2.60	2.61
	1.75	2.15	2.26
	6.75	2.55	2.42
	37.75	1.92	1.86
	53.25	2.68	2.31
	77.75	1.66	1.75
	95.75	2.25	2.31
	98.25	2.42	3.92
	107.75	2.34	2.52
	115.75	2.18	2.57
	130.25	2.81	2.82
	152.75	1.44	1.78
	162.25	2.69	1.74

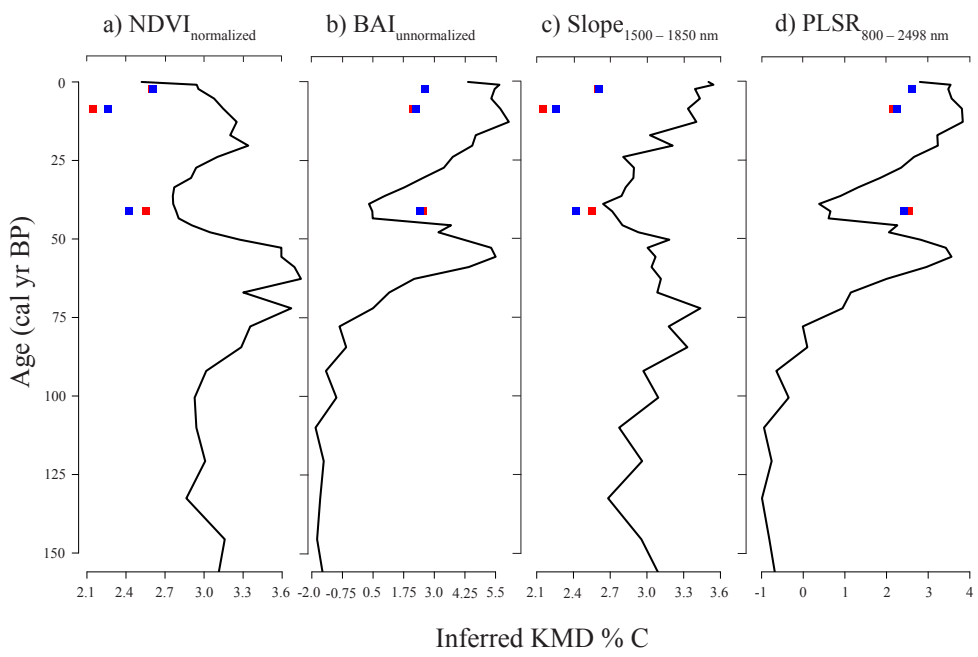

Figure 3.4. Recent (150 cal yr BP) black carbon reconstructions. Charcoal reconstructions from the top statistcally performing models: $NDVI_{normalized}$ (a), $BAI_{unnormalized}$ (b), $Slope_{1500 – 1850\ nm}$ (c), and $PLSR_{800 – 2498\ nm}$ (d) are converted to KMD % C for comparison to measured black carbon levels (red and blue boxes represent duplicate measurements).

sediment cores.

Applying the $Slope_{1500-1850\ nm}$ model to the composite core absorbance values and converting the results to KMD % C produces a black carbon reconstruction over the last 8000 cal yr BP (Figure 3.5a). KMD % C ranges from 0% at the Mazama ash layer to 4.32% at 5370 cal yr BP. Additional measurements of KMD % C indicate that spectroscopic estimates approximate measured black carbon concentration at specific intervals in the percussion core (Figure 3.5a, Table 3.3).

Cygnet Lake (44.65° N, 110.60° W; 2530 m asl; Millspaugh *et al.*, 2000) charcoal particle counts (particles • cm^{-2} • yr^{-1}) plotted alongside the Whitebark Moraine Pond data illustrate simultaneous peaks in the charcoal record and similar trends in overall charcoal loads within the GYE region (Figure 3.5b). Frequent, high particle count events dominate the Cygnet Lake record below approximately 4000 cal yr BP with a decrease in particle count peak sizes and frequency into the late Holocene (Figure 3.5b). Reconstructed KMD % C from Whitebark Moraine Pond exhibits similar trends in raw data with higher concentrations of black carbon before 4000 cal yr BP and a visible decrease thereafter (Figure 3.5a). Both records also reveal an increase in charcoal and black carbon concentrations in the last 300 years compared to late Holocene trends.

3.4.4. Reconstructed charcoal time series analysis

Cubic spline decomposition of the normalized KMD % C dataset, using alternately 250 year and 3000 year spans, enables the identification of positive anomalies from background black carbon levels (Figure 3.6). Both the 250 and 3000 year models detrend the normalized KMD % C data to highlight high and low frequency trends in the dataset, respectively (Figure 3.6a). Subtracting each

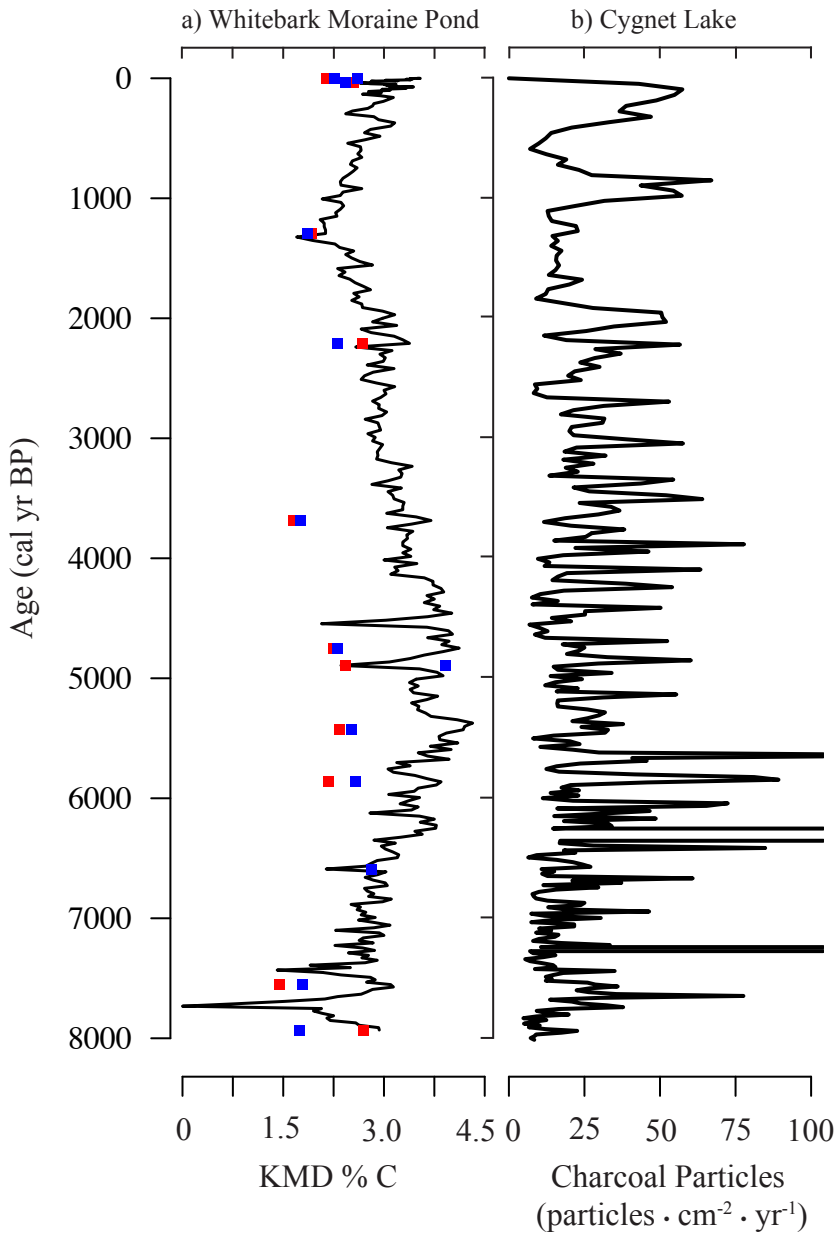

Figure 3.5. Whitebark Moraine Pond charcoal reconstruction comparison. A raw data comparison of KMD % C reconstruction from Whitebark Moraine Pond (a) and Cygnet Lake (b) charcoal particle counts (Millspaugh & Whitlock, 2000; Power *et al.*, 2008). Red and blue markers indicate % C levels measured from the composite core. Coincident peaks and valleys in the datasets indicate synchronous regional fire trends.

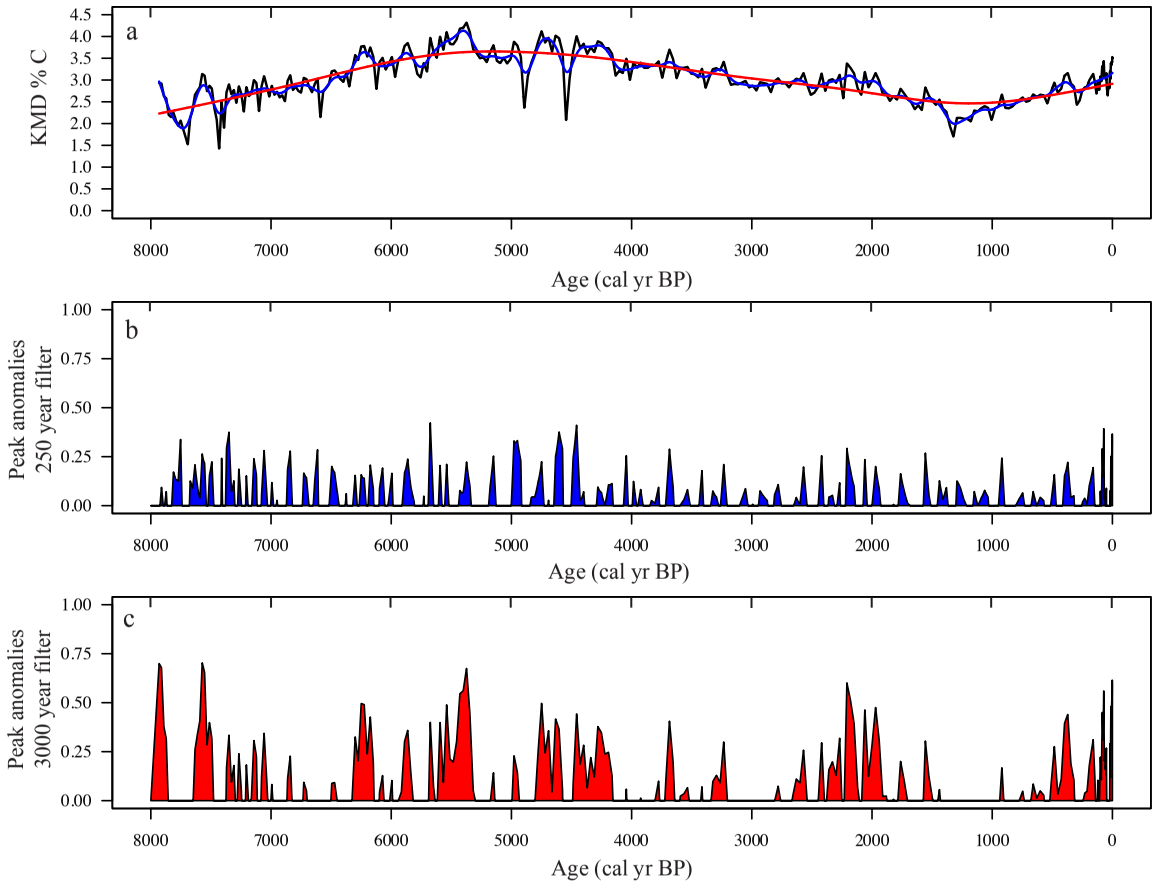

Figure 3.6. Whitebark Moraine Pond detrended charcoal data. The KMD % C reconstruction are fit with both the 250 year (blue line) and 3000 year (red line) filter cubic spline models (a). Positive anomalies from the 250 and 3000 year spline models are plotted as peaks in fire activity (b and c, respectively).

of the spline models from the raw KMD % C dataset emphasizes large fire events as peaks in sub-millennial and multi-millennial trends (3.6b-c). Exceedances from the 3000 year spline model, indicating severe perturbations from the multi-millennial background charcoal signal, averaged 8 fire events per millennium (fires/1000 yr) for 8000 – 4000 cal yr BP and 6 fires/1000 yr for 4000 – present (Figure 3.6c).

The two spline-detrended models of reconstructed KMD % C datasets were then subjected to wavelet analysis (Figure 3.7a,e). Two intervals encompassing the Mazama ash with anomalously low KMD % C and visible alterations to the sediments (155.75 − 156.25 cm) were removed from wavelet analysis to remove the influence of the Mazama tephra. The wavelet power spectrum tracks charcoal variance with periodicities reflecting the highest statistical power represented by the darkest red colors within the cone of influence (Figure 3.7b,f). For the 250 year spline model, the highest power resides in periodicities between 128 and 256 years with maximum power of 0.6 (Figure 3.7c). In the 3000 year spline model, periodicities between 128 and 2048 years produce the highest statistical power ranging from 1 to 3 (Figure 3.7g). Maximum variance is achieved at 4500 cal yr BP in both the 250 year and 3000 year spline models with variances approaching 0.06 and 0.05, respectively (Figure 3.7d,h). Of particular note in the 3000 year spline wavelet power spectrum analysis is the breakdown of higher periodicity events (512 to 1024 year periods) beginning at 4500 cal yr BP and extending into recent times.

The last 150 years displays a pronounced increase in fire activity in comparison to last two millennia (Figure 3.4c, 3.5a). Increases in peak size, width, and frequency of anomaly events from both the 250 year and 3000 year spline models differ considerably from anomaly patterns over the previous 2000 years (3.6b-c). Though these years lie near the edge of the cone of influence in

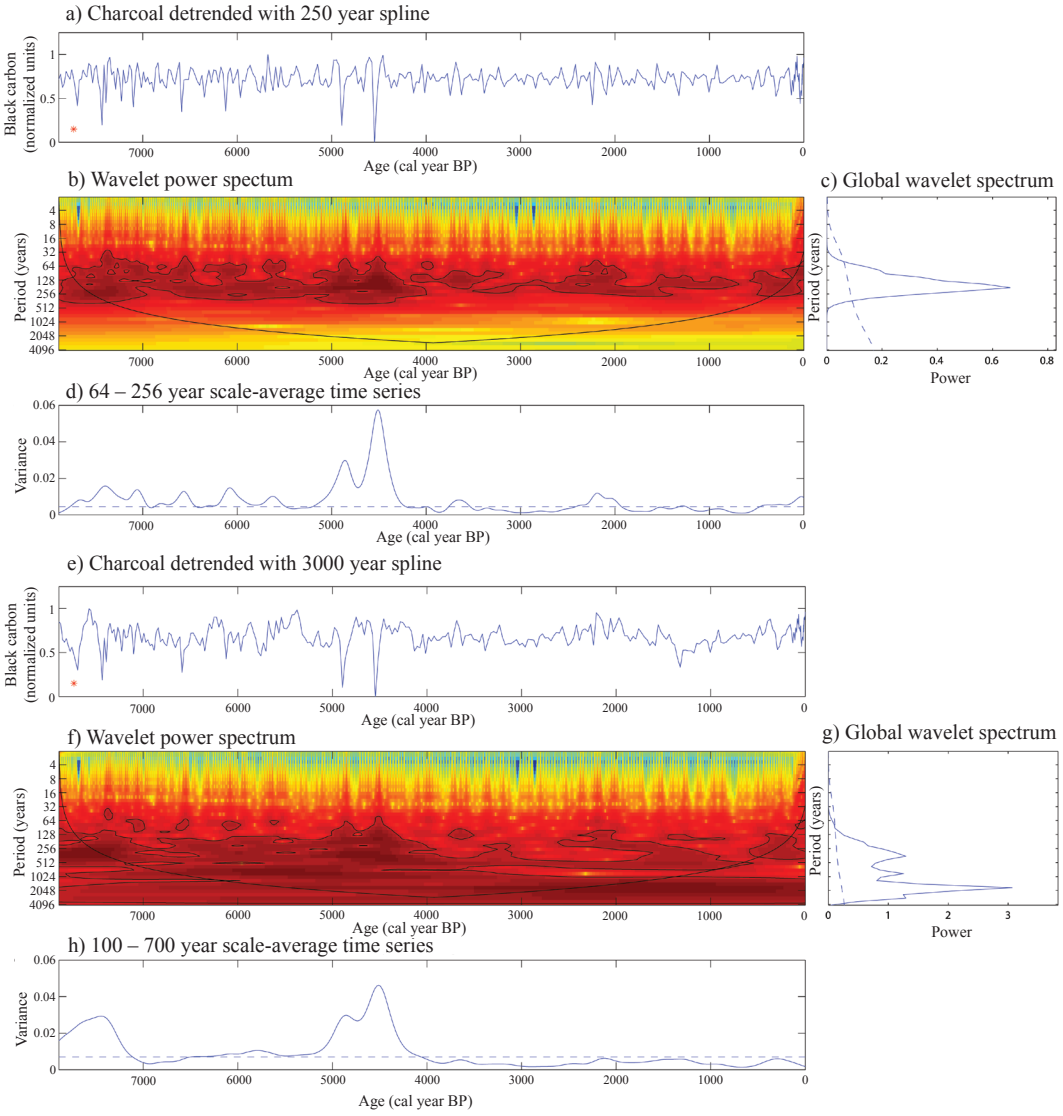

Figure 3.7. Whitebark Moraine Pond reconstructed charcoal wavelet analysis. The detrended 250 and 3000 year filter spline models (a, e), wavelet power spectrum (b, f), and global wavelet power spectrum (c, g, respectively) analyze statistically significant periodicities in the normalized KMD % C dataset. Two anomalously low % C data points, visibly affected by the Mazama ash layer, were removed from the wavelet analysis (denoted with red *; a, e). Periodicities of highest power are indicated by the darkest red colors (b, f). Panels (d) and (h) analyzed variance over time in the most powerful periodicities from the 250 year spline model (64 – 256 years) and in the 3000 year spline model (100 – 750 years), respectively.

the wavelet analysis, the statistically interpretable values reveal a strengthening of power in lower periodicity events (64 – 128 year) in black carbon detrended with the 250 year spline model (Figure 3.7b).

3.5. Discussion

3.5.1. Down-core spectroscopic variation and charcoal model selection

Absorbance patterns across the VNIR spectrum of the down-core samples mimic the sediment standard (0% charcoal) established in Chapter 2 (Figure 3.3a). However, particular spectroscopic features are not uniform between samples. Height, shape, and peak absorbance changes in the chlorophyll *a* feature vary independently with depth (Figure 3.3b), confirming our disinclination towards calibration models including this portion of the spectrum ($NDVI_{normalized}$ and $BAI_{unnormalized}$), as discussed in Chapter 2. The independent nature of the chlorophyll *a* peak throughout the core samples indicates a response to environmental conditions at the time of deposition, likely primary productivity and not specifically charcoal content (Michelutti *et al.*, 2005, 2010; Wolfe *et al.*, 2006). The OH features at approximately 1400 nm and 1900 nm do not display significant spectroscopic variations between samples (Figure 3.3a,e) but do respond to the progressive decrease in absorbance across the VNIR spectrum with increasing core depth. Neither direct reference of this effect nor potential causes has been gleaned from the relevant literature. We note likely triggers could arise from compaction and reduction in porosity with continued deposition in lake bottom environments. Further investigation of this effect should be undertaken.

The tendency of samples to exhibit an overall decrease in absorbance across VNIR wavelengths with increased depth is of particular importance to calibration efforts. Because absorbance measurements of most down-core samples fall below our 0% charcoal standard (Figure 3.3a), calibration models

inevitably reconstruct negative charcoal percentages, which in theory remains impossible with nearly constant background charcoal deposition after fire events (Whitlock & Millspaugh, 1996; Long *et al.*, 1998; Whitlock & Larsen, 2001; Marlon *et al.*, 2006; Higuera et al., 2007, 2010b; Conedera *et al.*, 2009). To avoid negative reconstructions, and to independently verify charcoal inclusion levels, the KMD % C conversion was calibrated. However, highly negative charcoal percentages generated from calibration models responding to the decrease in absorbance with depth still reconstruct negative black carbon concentrations ($BAI_{unnormalized}$ and $PLSR_{800-2498\ nm}$; Figure 3.4b,d). These calibration models must therefore be excluded from reconstruction efforts because of their inability to mitigate problems relating to absorbance changes with depth.

The $Slope_{1500-1850\ nm}$ model overcomes the down-core absorbance effect. The model is based on the incremental rise in linear slope coefficients as charcoal content increases within 1500 – 1850 nm, an otherwise spectrally benign region between the 1400 nm and 1900 nm OH features (Figure 3.3c). These changes in slope coefficients respond to charcoal concentrations, independent to absorbance decreases with increasing core depth or the behavior of OH bands (Figure 3.3d). This feature, as well as the smallest sum of residuals (3.77) in comparison to the other models converted to KMD % C, elevates $Slope_{1500-1850\ nm}$ to the highest performing charcoal calibration model. Consequently, the $Slope_{1500-1850\ nm}$ model is chosen for subsequent Holocene charcoal reconstructions.

3.5.2. Verification of Holocene fire reconstruction: KMD conversion and Cygnet Lake comparison

The composite sedimentary record from Whitebark Moraine Pond definitively tests the spectroscopic charcoal quantification technique through the reconstruction of Holocene charcoal variability. Conversion from inferred %

charcoal to KMD % C utilizes an independently verifiable metric that validates results from core samples, ensuring that the spectroscopically inferred charcoal percentages are in fact a consequence of charcoal inclusion and not darker mineral phases. Although not identical to inferred KMD % C, similar trends in measured KMD % C give confidence to spectroscopically-derived black carbon reconstructions from Whitebark Moraine Pond (Figure 3.5a). The high carbon recovery rate (98%) confirms digestion of less combusted charcoal phases from the KMD process does not generate the overall decrease of measured % C in comparison to spectroscopically inferred carbon percentages. Thus, the spectroscopic method generally overestimates included carbon percentages. Further refinement of both our calibration series could mitigate this problem, but at present the disparity between our measured *versus* reconstructed % C is not sufficient to disregard trends highlighted by spectroscopically inferred carbon levels.

Though measured KMD % C varies slightly from inferred KMD % C for the Holocene record (Figure 3.5a), overall trends in the sampled intervals confirm higher KMD % C levels throughout the mid Holocene, a decrease into the late Holocene, and subsequent rise to modern times. Decreases in inferred KMD % C after 4200 cal yr BP extend into the late Holocene. The slight rise in inferred KMD % C at 500 cal yr BP distinguishes a pronounced decrease in black carbon during the Little Ice Age (most visible at 300 cal yr BP) and accurately identifies the peak in black carbon associated with the 1988 Yellowstone National Park wildfires.

Correlation to regional charcoal datasets is an additional validation of spectroscopic black carbon reconstructions. Cygnet Lake in the Central Plateau of Yellowstone National Park provides an excellent analogue for regional paleofire and climatic trends with pollen and continuous (1 cm sampling interval) optically

counted macroscopic charcoal records from lake sediments encompassing the entire Holocene (Whitlock, 1993; Millspaugh *et al.*, 2000). Charcoal particle counts from Cygnet Lake are comparable to raw KMD % C reconstructions from Whitebark Moraine Pond (Figure 3.5b). Because of the local transport dynamics of macroscopic charcoal particles, we do not expect both records to be identical; however, frequency and size of particle count peaks from 8000 to 4200 cal yr BP, coincident with higher KMD % C levels, testify to the higher occurrence of fire events within the mid Holocene. The decreasing size and frequency of charcoal particle count peaks in Cygnet Lake between approximately 4200 to 1500 cal yr BP is also reflected in the Whitebark Moraine Pond record with a decrease in KMD % C. A relative increase in black carbon over the last millennium, with a notable rise in the last 500 years, is similarly illustrated with an increase in charcoal particles in Cygnet Lake over the same intervals. Differences in fire proxies, local fire conditions, and distance between sites (approximately 100 km) preclude identical fire reconstructions, but direct links in Holocene regional fire relationships are readily identifiable from the Whitebark Moraine Pond black carbon and Cygnet Lake charcoal particle count records, and are expected based on the physics of charcoal transport. Cygnet Lake comparisons and measured KMD % C confirm spectroscopically-inferred charcoal trends from Whitebark Moraine Pond, grounding Holocene fire reconstructions and inviting further paleofire frequency analyses from this continuous record.

3.5.3. Time series analysis; Holocene fire frequency

Traditional paleofire analyses deconstruct charcoal concentration data into distinct fire events, "signal," and continuously present background charcoal, "noise." Researchers attribute background charcoal to biomass changes, depositional processes, bioturbation, sedimentation rates, and reworking from

mass-wasting events (Millspaugh & Whitlock, 1995; Long *et al.*, 1998; Carcaillet *et al.*, 2001; Higuera *et al.*, 2010a, 2010b). Peaks above an established threshold value represent individual fire events or multiple fires occurring during a small time span. Fire frequency analyses rely upon background charcoal trends established through moving averages, locally weighted averages (LOWESS or LOESS), Gaussian mixture models, and other user-selected smoothing methods (e.g. Long *et al.*, 1998; Brunelle & Whitlock, 2003; Higuera *et al.*, 2010a, 2010b; Whitlock *et al.*, 2012). Over- or under-fitting data with incorrect polynomial smoothing functions, averaging window widths, and peak threshold levels interplay with input charcoal data, considerably affecting resultant fire frequency outputs and offering opportunities for researchers to adjust parameters such that frequency results adhere to *a priori* knowledge or assumptions.

In keeping with the exploratory nature of the project, we detrended the spectroscopically-derived charcoal data using a cubic polynomial spline to avoid problems associated with traditional decomposition techniques. Experiments with other detrending techniques such as LOESS smoothing and running means through the raw data yield similar results to the cubic spline, implying little sensitivity to the exact smoothing protocol used and strong underlying structure within the primary data.

The 250 and 3000 year cubic spline filters detrend charcoal data into high and low frequency trends, respectively (Figure 3.6a). Removal of the 250 year period spline model emphasizes higher frequency, centennial-scale fire events, appropriately reflecting more but smaller size peak anomalies in comparison to the peaks derived from the 3000 year filter, which distinguishes millennial-scale fire events (Figure 3.6b). ^{210}Pb dating attributes the last black carbon peak in both the 250 and 3000 year filter peak anomaly results to the 1988 Yellowstone wildfires. Utilizing the size of the 1988 peak, we can determine fire events of

similar size and severity (i.e. producing similar charcoal loads) occurred only three times in the region during the past 8000 years, irrespective of filter choice (Figure 3.6b-c). Our data supports previous conclusions that fires comparable to the 1988 Yellowstone wildfires have occurred within the mid-late Holocene in the GYE (Millspaugh & Whitlock, 1995; Millspaugh *et al.*, 2000, 2004; Huerta et al., 2009).

Increased size and frequency of peak anomalies prior to 4200 cal yr BP suggest a change in fire regime into the late Holocene (Figure 3.6b-c). An average of 8 fires/1000 yr drops to 6 fires/1000 yr after 4000 cal yr BP and 5 fires/1000 yr in the last two millennia. The threshold used to establish these counts was anomaly from the 3000 year spline model, unlike traditional decomposition methods that arbitrarily choose a threshold value for peak counts in addition to the subtraction of background charcoal model. Our method removes additional errors associated with supplementary *post hoc* data transformations while still maintaining the same regional fire frequency trends of Cygnet Lake (fire maxima of 15 fires/1000 yr at 9900 cal yr BP dropping to the present frequency of 2 – 3 fires/1000 yr). The lowest fire frequency of the entire Holocene (2 – 5 fires/1000 yr) has been noted over the past two millennia in Cygnet Lake, a trend that is mimicked in Whitebark Moraine Pond (Millspaugh *et al.*, 2000). Specific climatic forcing events causing the regional fire minima between 2000 – 1000 cal yr BP are still under investigation (Marlon *et al.*, 2006; Whitlock *et al.*, 2003, 2008).

Wavelet analysis further distinguishes 4200 cal year BP as a fire regime transition point. Power spectrum analyses of the 250 and 3000 year filtered datasets remove low-frequency secular trends from the charcoal dataset and allow us to analyze changes in fire event recurrence. The wavelet power spectrum ranks 64 – 256 year and 100 – 700 year periodicities at the highest statistical power,

respectively (Figure 3.7b,f). A marked breakdown of these periodicities by 4000 cal yr BP is easily visible by softer tones in the wavelet power spectrum of the 250 and 3000 year filters, indicating a shift in the fire regime. The continual collapse in power is marked by a hiatus in these periodicities visible at 500 cal yr BP in both filter models. Coincident timing of the changes in periodicity, irrespective of the filter utilized, attest to the underlying strength of the dataset and the reality of the signal.

A change in data structure within the last 150 years is highlighted in the raw Whitebark Moraine Pond black carbon data with increased peak size and frequency and strengthening of power in lower periodicities in the wavelet analysis (Figure 3.5a, 3.6b-c, 3.7b). Likely cause of this change in charcoal input despite human suppression to the fire system lies in the regional transport distance of our charcoal record. Though national parks actively suppressed fire from 1872 to 1972, regional fire activity still occurred, which the alpine catchment of Whitebark Moraine Pond faithfully reflects with subtle variations and more noticeable peaks in the 1860s, 1930s and a steady rise since 1988, fitting with regional fire occurrence (Houston, 1973; Loope & Gruell, 1973; Romme & Despain, 1989).

The termination of mid-Holocene fire trends at 4200 cal yr BP coincides with global climate trends that Walker *et al.* (2012) propose as defining the mid-late Holocene transition. Millspaugh *et al.* (2000) attribute a similar decrease in mid-late Holocene fire frequency from Cygnet Lake records to decreases in summer warmth and aridity from decreasing insolation effects after the Holocene insolation maximum (ca. 9900 cal yr BP). Whitebark Moraine Pond falls within the geographically-defined summer-dry precipitation regime and upholds the fire frequency trends typical of the area with the highest fire frequency synchronous to increased solar insolation. Decreases in fire frequency coincide with decreased

insolation throughout the late Holocene into modern times, promoting mature forest stands and the current trend of infrequent, stand-replacing fires (Millspaugh *et al.*, 2004; Whitlock *et al.*, 2008). Due to the cooler, wetter conditions than the mid Holocene and recently the effects of human fire suppression throughout the twentieth century, a dearth of fire has allowed fuels and biomass to accumulate, effectively creating a "fire deficit" for which only increased fire in the future can correct (Marlon *et al.*, 2012). With the current imbalance between fire occurrence and biomass, a notable increase in fire events is forecasted for the future, responding to the abundance of fuels and increased temperatures, summer drought, and length of fire season associated with the changing climate (Westerling et al., 2006, 2011; Whitlock *et al.*, 2008; Flannigan *et al.*, 2009; Romme *et al.*, 2011; Marlon *et al.*, 2012).

3.6. Conclusion

Spectroscopic analysis of lake sediment absorbance response to charcoal inclusions successfully reveals charcoal concentration information. The $Slope_{1500 - 1850\ nm}$ model most accurately predicts charcoal concentrations after conversion to KMD % C and comparison to measured black carbon levels. Paleofire reconstructions based on spectroscopically-derived charcoal records adhere to regional fire histories with highly resolved archives revealing additional fire frequency information in comparison to traditional optically-counted charcoal records. Time and resource savings from automated protocols, readily comparable metrics to black carbon measurements, and the potential to glean additional information from the sedimentary record attest to the benefits of using environmental spectroscopy for paleofire determination.

3.7. References

Blaauw, M. 2010. Methods and code for 'classical' age-modeling of radiocarbon sequences. Quaternary Geochronology: 1-7.

Brunelle, A. & Whitlock, C. 2003. Postglacial fire, vegetation, and climate history in the Clearwater range, northern Idaho, USA. Quaternary Research 60: 307-318.

Carcaillet, C., Bouvier, M., Fréchette, B., Larouche, A.C., Richard, P.J.H. 2001. Comparison of pollen-slide and sieving methods in lacustrine charcoal analyses for local and regional fire history. The Holocene 11: 467-476.

Cook, E.R & Peters, K. 1981. The smoothing spline: a new approach to standardizing forest interior tree-ring width series for dendroclimatic studies. Tree-Ring Bulletin 41: 45-53.

Conedera, M., Tinner, W., Neff, C., Meurer, M., Dickens, A.F., Krebs, P. 2009. Reconstructing past fire regimes: methods, applications, and relvance to fire management and conservation. Quaternary Science Reviews 28: 555-576.

Glew, J.R. 1991. Miniature gravity corer for recovering short sediment cores. Journal of Paleolimnology 5: 285-287.

Flannigan, M.D., Krawchuk, M.A., de Groot, W.J., Wotton, B.M., Gowman, L.M. 2009. Implications of changing climate for global wildland fire. International Journal of Wildland Fire 18: 483-507.

Higuera, P.E., Gavin, D.G. Bartlein, P.J. Hallett, D.J. 2010a. Peak detection in sediment-charcoal records: impacts of alternative data analysis methods on fire-history interpretations. International Journal of Wildland Fire 19: 996-1014.

Higuera, P.E., Whitlock, C., Gage, J.A. 2010b. Linking tree-ring and sediment charcoal records to reconstruct fire occurrence and area burned in

subalpine forests of Yellowstone National Park, USA. The Holocene: DOI: 10.1177/0959683610374882.

Higuera, P.E., Peters, M.E., Brubaker, L.B., Gavin, D.G. 2007. Understanding the origin and analysis of sediment-charcoal records with a simulation model. Quaternary Science Reviews 26: 1790-1809.

Houston, D.B. 1973. Wildfires in Northern Yellowstone National Park. Ecology 54: 1111-1117.

Huerta, M.A., Whitlock, C., Yale, J. 2009. Holocene vegetation-fire-climate linkages in northern Yellowstone National Park, USA. Palaeogeography, Palaeoclimatology, Palaeoecology 271: 170-181.

Kurth, V.J., MacKenzie, M.D., DeLuca, T.H. 2006. Estimating charcoal content in forest mineral soils. Geoderma 137: 135-139.

Laird, L.D. & Campbell, I.D. 2000. High resolution palaeofire signals from Christina Lake, Alberta: a comparison of the charcoal signals extracted by two different methods. Palaeogeography, Palaeoclimatology, Palaeoecology 164: 111-123.

Long, C.J., Whitlock, C., Bartlein, P.J., Millspaugh, S.H. 1998. A 9000-year fire history from the Oregon Coast Range, based on a high-resolution charcoal study. Canadian Journal of Forest Research 28: 774-787.

Loope, L.L. & Gruell, G.E. 1973. The ecological role of fire in the Jackson Hole area, northwestern Wyoming. Quaternary Research 3: 425-443.

Marlon, J.R., Bartlein, P.J., Gavin, D.G., Long, C.J., Anderson, R.S., Briles, C.E., Brown, K.J., Colombaroli, D., Hallett, D.J., Power, M.J., Scharf, E.A., Walsh, M.K. 2012. Long-term perspective on wildfires in the western USA. Proceedings of the National Academy of Sciences 109: E535-E543.

Marlon, J., Bartlein, P.J., Whitlock, C. 2006. Fire-fuel-climate linkages in the northwestern USA during the Holocene. The Holocene 16: 1059-1071.

Michelutti, N., Blais, J.M., Cumming, B.F., Paterson, A.M., Rühland, K., Wolfe, A.P., Smol, J.P. 2010. Do spectrally inferred determinations of chlorophyll a reflect trends in lake trophic status? Journal of Paleolimnology 43: 205-217.

Michelutti, N., Wolfe, A.P., Vinebrooke, R.D., Rivard, B., Briner, J.P. 2005. Recent primary production increases in arctic lakes. Geophysical Research Letters 32: L19715, doi:10.1029/2005GL023693.

Millspaugh, S.H. & Whitlock, C. 1995. A 750-year fire history based on lake sediment records in central Yellowstone National Park. USA. The Holocene 5: 283-292.

Millspaugh, S.H., Whitlock, C., Bartlein, P.J. 2000. Variations in fire frequency and climate over the past 17000 yr in central Yellowstone National Park. Geology 28: 211-214.

Millspaugh, S.H., Whitlock, C., Bartlein, P.J., 2004. Postglacial fire, vegetation, and climate history of the Yellowstone-Lamar and Central Plateau provinces, Yellowstone National Park. In: Wallace, L. (Ed.), After the Fires: The Ecology of Change in Yellowstone National Park. Yale University Press: 10-28.

Power, M.J., Marlon, J., Ortiz, N., Bartlein, P.J., Harrison, S.P., Mayle, F.E., Ballouche, A., Bradshaw, R., Carcaillet, C., Cordova, C., Mooney, S., Moreno, P., Prentice, I.C., Thonicke, K., Tinner, W., Whitlock, C., Zhang, Y., Zhao, Y., Anderson, R.S., Beer, R., Behling, H., Briles, C., Brown, K.J., Brunelle A., Bush, M., Camill, P., Chu, G.Q., Clark, J., Colombaroli, D., Connor, S., Daniels, M., Daniau, A.-L., Dodson, J., Doughty, E., Edwards, M.E., Fisinger, W., Foster, D., Frechette J., Gaillard, M.-J., Gil-Romera, G. Gavin, D.G., Gobet, E., Haberle, S., Hallett, D.J., Higuera, P., Hope, G., Horn, S., Impagliazzo, S., Inoue, J., Kaltenrieder, P., Kennedy, L., Kong,

Z.C., Larsen, C., Long, C.J., Lynch, J., Lynch, B., McGlone, M., Meeks, S., Mensing, S., Meyer, G., Minckley, T., Mohr, J, Nelson, D., New, J., Newnham, R., Noti, R., Oswald, W., Pierce, J., Richard, P.J.H., Rowe, C., Sanchez Goñi, M.F., Shuman, B.J., Takahara, H., Toney, J., Turney, C., Umbanhower, C., Vandergoes, M., Vanniere, B., Vescovi, E., Walsh, M., Wang, X., Williams, N., Wilmshurst, J., Zhang , J.H.. 2008. Changes in fire regimes since the Last Glacial Maximum: an assessment based on a global synthesis and analysis of charcoal data. Climate Dynamics, Vol. 30, No. 7-8, pp. 887-907, June 2008. [DOI 10.1007/s00382-007-0334-x].

Ramsey, C.B. 2001. Development of the radiocarbon calibration program OxCal. Radiocarbon 43: 355-363.

Reimer, P.J., Baillie, M.G.L., Bard, E., Bayliss, A., Beck, J.W., Blackwell, P.G., Ramsey, C.B., Buck, C.e., Burr, G.S., Edwards, R.L., Friedrich, M., Grootes, P.M., Guilderson, T.P., Hajdas, I., Heaton, T.J., Hogg, A.G, Hughen, K.A., Kaiser, K.F., Kromer, B., McCormac, F.G., Manning, S.W., Reimer, R.W., Richards, D.A., Southon, J.R., Talamo, S., Turney, C.S.M., van der Plicht, J., Weyhenmeyer, C.E. 2009. IntCal09 and Marine09 radiocarbon age calibration curves, 0-50,000 years cal BP. Radiocarbon 51: 1111-1150.

Romme, W.H., Boyce, M.S., Gresswell, R., Merril, E.H., Minshall, G.W., Whitlock, C., Turner, M.G. 2011. Twenty years after the 1988 Yellowstone fires: Lessons about disturbance and ecosystems. Ecosystems: DOI: 10.1007/s10021-011-9470-6.

Romme, W.H. & Despain, D.G. 1989. Historical perspective on the Yellowstone fires of 1988. BioScience 39: 695-699.

Tinner, W. & Hu, F.S. 2003. Size parameters, size-class distribution and area-number relationship of microscopic charcoal: relevance for fire

reconstruction. The Holocene 13: 499-505.

Torrence, C. & Compo, G.P. 1998 A practical guide to wavelet analysis. Bulletin of the American Meteorological Society 79: 61-78.

Walker, M.J.C., Berkelhammer, M., Björch, S., Cwynar, L.C., Fisher, D.A., Long, A.J., Lowe, J.J. Newham, R.M., Rasmussen, S.O., Weiss, H. 2012. Formal subdivision of the Holocene Series/Epoch: a discussion paper by a working group of INTIMATE (Integration of ice-core, marine and terrestrial records) and the Subcommission on Quaternary Stratigraphy (International Commission on Stratigraphy). Journal of Quaternary Science 27: 649-659.

Westerling, A.L., Hidalgo, H.G., Cayan, D.R., Swetnam, T.W. 2006. Warming and earlier spring increase western U.S. forest fire activity. Science 313: 940-943.

Westerling, A.L., Turner, M.G. Smithwick, E.A.H., Romme, W.H., Ryan, M.G. 2011. Continued warming could transform Greater Yellowstone fire regimes by mid-21st century. Proceedings of the National Academy of Sciences 108: 13165-13170.

Whitlock, C. 1993 Postglacial vegetation and climate of Grand Teton and southern Yellowstone National Parks. Ecological Monographs 63: 173-198.

Whitlock, C., Bartlein, P.J., Marlon, J. Brunelle, A., Long, C. 2003. Holocene fire reconstructions from the Northwestern U.S.: an examination at multiple time scales. Second International Wildland Fire Ecology and Fire Management Congress (extended abstract): 4C.1-5. <http://ams.confex.com/ams/pdfpapers/66514.pdf>

Whitlock, C., Dean, W.E., Fritz, S.C., Stevens, L.R., Stone, J.R., Power, M.J., Rosenbaum, J.R., Pierce, K.L., Bracht-Flyr, B.B. 2012. Holocene

variability inferred from multiple proxy records from Crevice Lake, Yellowstone National Park, USA. Palaeogeography, Palaeoclimatology, Palaeoecology 331: 90-103.

Whitlock, C. & Larsen, C. 2001. Charcoal as a fire proxy. In Tracking Environmental Change Using Lake Sediments: Volume 3 Terrestrial, Algal, and Siliceous indicators; Smol, J.P., Birks, H.J.B., and Last. W.M. Kluwer Academic Publishers, Dordrecht: 75-97.

Whitlock, C., Marlon, J., Briles, C., Brunelle, A., Long, C., Bartlein, P. 2008. Long-term relations among fire, fuel, and climate in north-western US based on lake-sediment studies. International Journal of Wildland Fire 17: 72-83.

Whitlock, C. & Millspaugh, S.H. 1996. Testing the assumptions of fire-history studies: An examination of modern charcoal accumulation in Yellowstone National Park, USA. Holocene 6: 7-16.

Wolfe, A.P., Vinebrooke R.D., Michelutti N., Rivard B., Das B. 2006. Experimental calibration of lake-sediment spectral reflectance to chlorophyll a concentrations: methodology and paleolimnological validation. Journal of Paleolimnology 36: 91-100.

Zdanowicz, C.M., Zielinski, G.A., Germani, M.S. 1999. Mount Mazama eruption: Calendrical age verification and atmospheric impact assessed. Geology 27: 621-624.

CHAPTER 4

SUMMARY, CONCLUSIONS, AND RECOMMENDATIONS FOR FUTURE RESEARCH

4.1. Synthesis

The sedimentary record chronicles the interdependent relationships between fire, climate, and vegetation that vary on both short and long timescales. Sedimentary charcoal analyses reveal local to regional scale fire histories, but traditional methods of charcoal quantification are expensive and time-consuming. These shortfalls limit the number of sites ultimately available to differentiate regional fire signals from localized events superimposed upon larger climate-driven phenomena. By spectroscopically analyzing the <125 μm fraction of sediments using calibration tools for total charcoal content, a new procedure is now available for generating temporally continuous time-series of fire events. Comparison with regional Holocene records generated by traditional approaches not only demonstrates the great potential of spectroscopic approaches, but also adds further to the understanding of Holocene fire dynamics in the greater Yellowstone ecosystem.

4.1.1. Regional climate context

Extensive studies in the broader northern Rocky Mountain region reveal that two climatic sub-regions exist and are delineated by precipitation regimes (Whitlock & Bartlein, 1993). A balance between the northeast Pacific subtropical high-pressure system and monsoonal circulation patterns dominates the modern climate of the American western states (Tang & Reiter, 1984). Previous charcoal studies have focused on Cygnet Lake (2530 m asl) in central Yellowstone

National Park as well as Burnt Knob Lake (2250 m asl) in the Bitterroot Range (Figure 4.1a), which experience aridity due to the persistence of the northeast Pacific subtropical high-pressure system, consequently identified as sites having a "summer-dry" regime (Millspaugh *et al.*, 2000; Whitlock *et al.*, 2003; Millspaugh *et al.*, 2004). Slough Creek Lake (1884 m asl) in northern Yellowstone National Park, Baker Lake (2300 m asl) on the east slope of the Bitterroot Range, and Pintlar Lake (1921 m asl) are termed "summer-wet" because a summer monsoonal circulation pattern dominates the area, resulting in higher precipitation (Figure 4.1a; Whitlock *et al.*, 2003; Brunelle *et al.,* 2005). The spatial distribution of modern precipitation regimes appears to have persisted throughout the Holocene (Whitlock *et al.*, 1995). However, elevated summer insolation in the early to mid Holocene amplified the differences between these two climate regimes, resulting in the summer-dry region becoming more arid and summer-wet becoming wetter during the insolation maximum (Whitlock *et al.*, 2003).

4.1.2. Holocene fire: regional trends

These distinct precipitation patterns dictate fire and vegetation responses and are thus reflected within the individual lake records. Summer-wet sites record anomalously low fire activity at the solar insolation maxima and an increase in fire as summer insolation declines to modern levels (Figure 4.1b). Conversely, summer-dry sites experience the highest fire activity during the insolation maximum, decreasing thereafter (Figure 4.1c; Millspaugh *et al.*, 2000; Whitlock *et al.*, 2003; Millspaugh *et al.*, 2004; Brunelle *et al.*, 2005).

At the highest elevation (2800 m asl), the Whitebark Moraine Pond spectroscopic charcoal record contains elements that are present in both the summer-wet and summer-dry climate regimes (Figure 4.1d). The 3000 year cubic spline model was chosen for comparison purposes to emphasize the multi-

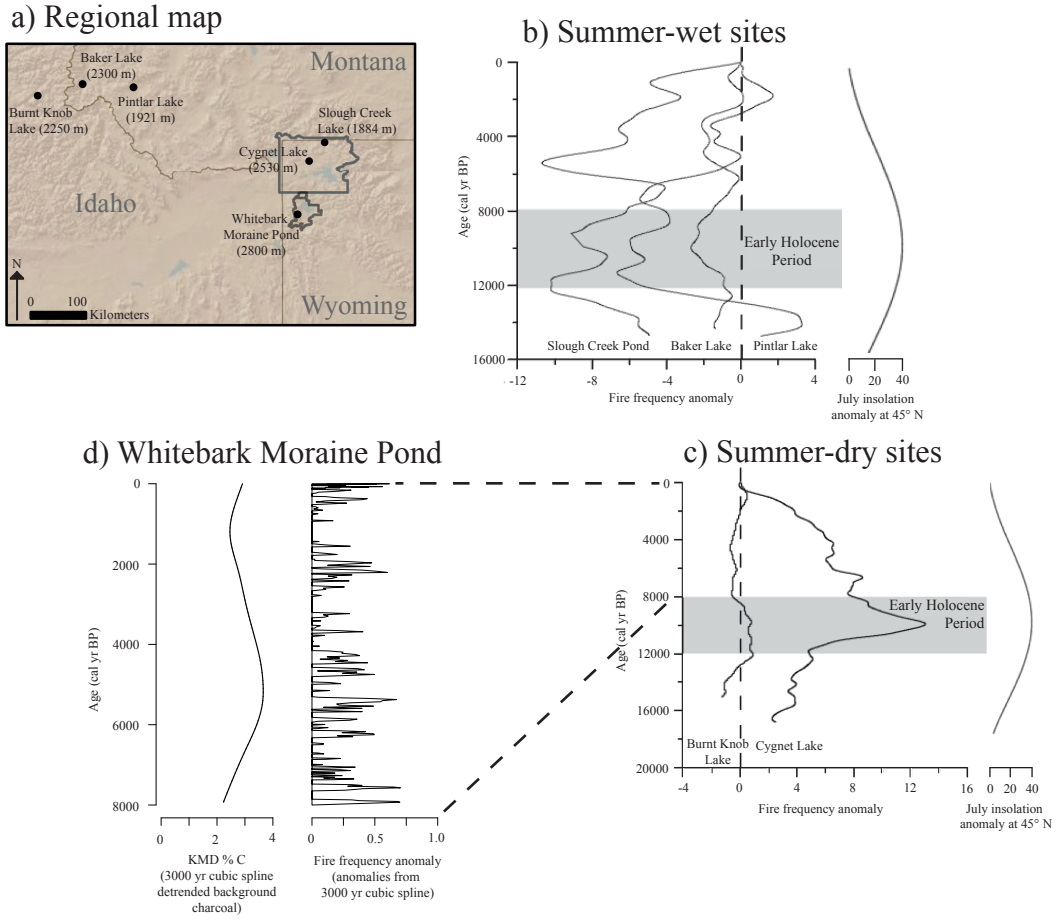

Figure 4.1. Regional fire synthesis. Regional map identifies each lake across northern Rocky Mountains (a). Fire trends differ dramatically in lakes from summer-wet (b) and summer-dry (c) sites within the northwestern Rocky Mountains across the Holocene (Millspaugh & Whitlock, 2000; Brunelle *et al.*, 2005; Power *et al.*, 2008). Whitebark Moraine Pond (d) summarizes both trends with high fire in the mid Holocene and highlighting the decrease at 2000 cal yr BP.

millennial trends in fire occurrence, opposed to the 250 year filter that allows centennial-scale events to convolute longer term trends. Although the Whitebark Moraine Pond record commences after the solar insolation maximum, a peak in fire activity is nonetheless evident in the mid Holocene (8000 – 6000 cal yr BP), highlighting an intermediate response between summer-wet and summer-dry sites. We suggest that this signature represents the more regional nature of the spectroscopically derived charcoal signal, implying that the spectroscopic methodology offers potentially new insights into understanding the broad scale response of fire to Holocene climate change. The larger, more regional source area of the Whitebark Moraine Pond record owes to the lake elevation, the highest of all the lakes in comparison, and the spectrum of charcoal analyzed (<125 μm).

The climax of the Whitebark Moraine Pond fire activity peak at 5500 cal yr BP lags slightly behind the other records, probably resulting from the regional transport dynamics of charcoal. We note that extending the Whitebark Moraine Pond record into the early Holocene remains necessary to fully capture the site's response during the summer insolation maximum. Declining charcoal concentrations after 2000 cal yr BP are witnessed in sites from both precipitation regimes (Figure 4.1b-c), and in Whitebark Moraine Pond with a minimum at 1500 cal yr BP (Figure 4.1d). Charcoal studies spanning the western American states produce a similar result (Whitlock *et al.*, 2003, 2008; Marlon *et al.*, 2006).

Summarily, the Whitebark Moraine Pond charcoal record captures a regionally coherent fire response to Holocene climate evolution, and thus appears to filter local-scale variations effectively. Current procedures for assessing regional fire activity involve biases associated with microscopic charcoal determinations that are rarely stratigraphically continuous due to the efforts involved, which hampers the accuracy of resultant fire frequency analyses. For this reason, multiple sites need to be compiled, which inevitably overemphasizes

local fire events despite statistical decomposition efforts. Thus, potentially skewed perceptions of regional fire trends can be partially obviated by spectroscopic quantifications of lake sediment charcoal.

4.2. Strengths and potentialities

The Whitebark Moraine Pond Holocene fire reconstruction attests to the benefits of spectroscopy for paleofire determination. However, automation, time and resource savings, and additional fire frequency information from continuous analyses are not the only advantages afforded by spectroscopic analysis of lake sediments. Table 4.1 compares spectroscopic and traditional charcoal determination methods more exhaustively, highlighting the manner in which each technique addresses issues inherent in charcoal analysis from lake sediments. As evidenced by the numerous drawbacks of traditional charcoal quantification procedures, current paleoanthracologic methodologies are enhanced by the advantages offered by spectroscopy.

The underlying benefit of the spectroscopic method relative to traditional charcoal quantification techniques is the minor amount of laboratory sample processing prior to analysis. Thus, sediments measured directly for absorbance represent an inherently more inclusive fraction than that having survived acetolysis and hydrofluoric acid pre-treatment. Calibration of sediment absorbance to amended charcoal additions, and subsequent conversion to total KMD black carbon concentrations, are based on simple yet powerful statistical relationships that predict measured charcoal values with considerable skill.

Finally, and most importantly for fire history trends, our charcoal decomposition method utilizes positive anomalies from simple cubic spline models to distinguish discrete fire events from background charcoal levels in a stratigraphically continuous record. This procedure accurately depicts variations

Table 4.1. Charcoal methodology comparison.

Issue	Traditional charcoal methods	Spectroscopic method
Charcoal source area	Different methods represent some or all of theoretical fire distances: local, extra-local, regional, and global	Includes all charcoal <125µm: regional and more distant source area
Charcoal signal decomposition	Fire frequency results heavily dependant upon background charcoal and peak threshold establishment techniques	Simple cubic spline models minimize *post hoc* statistical alteration of primary datasets for background charcoal and peak determination
Charcoal misidentification	Potential to misidentify dark minerals as charcoal fragments, especially in the smallest size fractions (i.e. pollen slide methods)	Misidentification of dark minerals, organics, or sediment inclusions possible, especially if down-core lithologic changes encountered
Charcoal burn conditions	Degree of carbonization alters charcoal appearance requiring protocol establishment when range of charcoals encountered (potential bias source)	Potentially affect absorbance depending on spectrum of burn conditions
Interstudy comparison	Different methods produce data as various metrics that require *post hoc* data transformations; laboratory technique differences using the same method complicate laboratory to laboratory comparisons	Charcoal calibrations unique to each lake; one metric (weight % charcoal) easily compared between analyses
Site selection	More viable sites	Charcoal recalibration needed for multiple sites; sediment lithology absorbance effects must be considered prior ot site selection
Analysis time	Prolonged sample preparation and analysis time	Quick analyses: approximately 1 minute per sample
Sampling frequency	Lengthy sample preparation procedures preclude continuous sampling for most methods	Continuous sampling easy
Sample fate	Destructive methodologies prevent multiple analyses on same samples	Non-destructive methodologies allow multiple analyses to be performed on the same samples
Reproducibility of primary data	Destructive methodologoies prevent re-analysis	Re-scanning of original samples easy and efficient
Temporal scale	Modern to Tertiary records	Only Holocene record tested at present
Temporal resolution	Annual to millennial records	Multi-decadal resolution available at present
Fire type determination	Particular methods better reflect certain fire types (i.e. infrequent, large fires vs frequent, small fires)	All types of fire equally represented because opacity of charcoal
Laboratory equipment requirements	Depending on method, expensive equipment (microscopes, imaging machines, measuring tools, etc.) and powerful chemical solvents	Freeze-drier, spectroradiometer, and freely available statistical software
Laboratory technician experience requirements	Years of training required before efficient and reliable charcoal identification possible; potential for human error ever-present	Automated methods minimize human errors and minimal experience required to perform sample preparation and measuring techniques

in the charcoal record due to higher charcoal concentrations, avoids excessive statistical reworking of primary data such as smoothing and interpolation, and circumvents biases associated with assigning arbitrary thresholds for fire identification from the record. Though spectroscopy commonly relies on statistics to deconvolute complex patterns, the example of charcoal, in which opacity is "blanketed" uniformly on the sediment matrix, is comparatively straight-forward: simple linear models are capable of detecting a robust charcoal signal from sediment absorbance values.

4.3. Concerns and potential pitfalls

Excluding larger fractions of charcoal (>125 μm) is necessary to prevent distortion of sediment absorbance signal due to particle size effects, but also prevents the spectroscopic method from procuring a local fire signal (Clark, 1988a, 1988b; Whitlock & Millspaugh, 1996; Long *et al.*, 1998; Clark, 1999). Thus, the spectroscopic method is unlikely to supplant traditional methods where strictly local fire reconstructions are sought, but rather may be used in combination to such methods to obtain a regional fire signal prior to sample processing. Also, the regional fire trend established spectroscopically may better determine background charcoal levels and improve threshold establishment for local fire identification.

The $\text{Slope}_{1500-1850\ \text{nm}}$ method, and all investigated calibration models, rely upon the opacity of pyrogenic carbon to amplify absorbance spectra of sediments with increasing charcoal concentration, yielding detectable spectroscopic patterns in the VNIR bands. This dependence on opacity may be confounded when lake sediments include dark minerals or organic phases, and/or where there is considerable down-core lithologic variability. Careful pre-selection of cores for analysis may obviate such problems, noting that Whitebark Moraine

Pond sediments are highly homogeneous. The influence of down-core matrix heterogeneity on spectroscopically-inferred charcoal needs to be fully explored in the future, although preliminary results from Ramshead Lake and Whitebark Moraine Pond (Chapter 2) suggest these issues may be tractable.

For our investigation, we established a sediment standard (0% charcoal) from a homogenous mixture of sediments taken from either lake with the assumption that they necessarily represent no or low charcoal because of the lack of recent fire activity within the watersheds. Although recent fires have not occurred, sediments still contain a baseline charcoal load due to reworking, specifically from the 1988 Yellowstone wildfires, and thus the 0% baseline is likely a minimum estimate of actual charcoal content. No matter the anchoring point for the charcoal calibration, we establish that current charcoal loads remain elevated in comparison to late Holocene charcoal levels, especially compared to the minima reached 2000 – 1000 cal yr BP (Figure 4.1d). The impossibility of attaining a sediment standard that truly reflects 0% charcoal forces us to recognize that our charcoal scale produces a fire record relative to present charcoal loads, which might be overly simplistic. However, with respect to conceptualizing Holocene climate and fire co-evolution in relation to present conditions, the inferences of this study are not compromised.

We note that the charcoal used for calibration originated from trees burned in 1988, and assumed to be representative of Holocene charcoals. However, this material comprises both larger and more angular fragments on average, have greater preserved xylotomy, and are, under light microscopy, more "brown" than "black" (Figure 2.3). At this point, we cannot know the specific effect of these differences, but similarities in absorbance patterns between charcoal specimens (Figure 2.4a) support their use in modeling the blanketing opacity charcoal imparts on sediments to relate charcoal concentrations to sediment absorbance

values, and thus fire events. The reliance on general opacity should not preferentially skew results towards specific charcoal of certain burn conditions, but this effect requires further investigation for definitive conclusions.

4.4. Recommendations for future studies

Facets of this project that could benefit from future study include, but are not limited to, the down-core absorbance problem associated with variable lithology, mid-infrared explorations of charcoal and lake sediment spectroscopic behavior, calibration of absorbance and conversions to KMD % C, and more explicit determinations of the spatial scales captured by conventional and spectroscopic fire frequency reconstructions. The progressive drop in background sediment absorbance with increasing depth in the core is of particular concern with respect to calibration procedures based on surface sediments. The method that best overcomes this problem is the $Slope_{1500-1850\ nm}$ approach, which bodes well for the general procedure but may also limit further refinement of this technique. Sediment compaction, differences in porosity, and diagenetic alterations are additional potential sources of influence on sediment absorbance unrelated to charcoal load, and these spectroscopic effects require additional study.

Continuing to explore the spectroscopic behavior of both sediment and charcoal within the mid-infrared spectral range (2500 – 25000 nm) could provide additional information regarding the molecular vibration and thus chemical bonding structure of our samples (Bellon-Maurel & McBratney, 2011). Bolstering the number of samples used for both the sediment:charcoal dilution series and the KMD conversion would strengthen both calibration efforts. The initial models predict that sediment charcoal inclusions lie between 0 – 0.5% charcoal; increasing the number of calibration samples within this specific

range, and subsequently refining calibration at lower ranges (<5% and even 1% charcoal) will considerably improve charcoal predictions from absorbance values. Lastly, a firmer basis for understanding charcoal particle motion dynamics in the atmosphere would allow more conclusive determination of charcoal transport distances inferred from the spectroscopic technique.

4.5. Conclusion

Understanding Holocene fire regimes, forcing mechanisms, and resultant ecological responses is vital in this time of rapidly changing climate. Our comprehension and subsequent management of potentially increased wildfire threats relies upon our ability to analyze and to understand past fire dynamics. As we approach the limits of climate variability typical of the Holocene, paleofire study needs to incorporate a record temporally sufficient to reflect the Holocene in its entirety, which only sedimentary charcoal archives provide. Protracted laboratory techniques, error sources inherent to counting methods, and statistical treatments plague interpretations based on traditional sedimentary charcoal analyses. This thesis offers an alternate approach to paleoanthracology that benefits from objectivity, automation, and rapid data generation, all afforded by spectroscopic analysis of sedimentary materials. The novel procedure for sedimentary charcoal quantification may provide a more detailed understanding of fire–climate–vegetation dynamics, and facilitate timely management decisions by improving the understanding of fire dynamics.

4.6. References

Bellon-Maurel, V. & McBratney, A. 2011. Near-infrared (NIR) and mid-infrared (MIR) spectroscopic techniques for assessing the amount of carbon stock in soils – Critical review and research perspectives. Soil Biology & Biochemistry 43: 1398-1410.

Brunelle, A., Whitlock, C., Bartlein, P., Kipfmueller, K. 2005. Holocene fire and vegetation along environmental gradients in the Northern Rocky Mountains. Quaternary Science Reviews 24: 2281-2300.

Clark, J.S. 1988a. Particle Motion and the Theory of Charcoal Analysis: Source Area, Transport, Deposition, and Sampling. Quaternary Research 30: 67-80.

Clark, J.S. 1988b. Stratigraphic charcoal analysis on petrographic thin sections: application to fire history on Northwestern Minnesota. Quaternary Research 30: 81-91.

Clark, R.N. 1999. Spectroscopy of Rocks and Minerals, and Principles of Spectroscopy. In Manual of Remote Sensing: Volume 3 Remote Sensing for the Earth Sciences; Rencz, A.N. John Wiley and Sons, New York: 3-58.

Long, C.J., Whitlock, C., Bartlein, P.J., Millspaugh, S.H. 1998. A 9000-year fire history from the Oregon Coast Range, based on a high-resolution charcoal study. Canadian Journal of Forest Research 28: 774-787.

Millspaugh, S.H., Whitlock, C., Bartlein, P.J. 2000. Variations in fire frequency and climate over the past 17000 yr in central Yellowstone National Park. Geology 28: 211-214.

Millspaugh, S.H., Whitlock, C., Bartlein, P.J., 2004. Postglacial fire, vegetation, and climate history of the Yellowstone-Lamar and Central Plateau provinces, Yellowstone National Park. In: Wallace, L. (Ed.), After

the Fires: The Ecology of Change in Yellowstone National Park. Yale University Press: 10-28.

Power, M.J., Marlon, J., Ortiz, N., Bartlein, P.J., Harrison, S.P., Mayle, F.E., Ballouche, A., Bradshaw, R., Carcaillet, C., Cordova, C., Mooney, S., Moreno, P., Prentice, I.C., Thonicke, K., Tinner, W., Whitlock, C., Zhang, Y., Zhao, Y., Anderson, R.S., Beer, R., Behling, H., Briles, C., Brown, K.J., Brunelle A., Bush, M., Camill, P., Chu, G.Q., Clark, J., Colombaroli, D., Connor, S., Daniels, M., Daniau, A.-L., Dodson, J., Doughty, E., Edwards, M.E., Fisinger, W., Foster, D., Frechette J., Gaillard, M.-J., Gil-Romera, G. Gavin, D.G., Gobet, E., Haberle, S., Hallett, D.J., Higuera, P., Hope, G., Horn, S., Impagliazzo, S., Inoue, J., Kaltenrieder, P., Kennedy, L., Kong, Z.C., Larsen, C., Long, C.J., Lynch, J., Lynch, B., McGlone, M., Meeks, S., Mensing, S., Meyer, G., Minckley, T., Mohr, J, Nelson, D., New, J., Newnham, R., Noti, R., Oswald, W., Pierce, J., Richard, P.J.H., Rowe, C., Sanchez Goñi, M.F., Shuman, B.J., Takahara, H., Toney, J., Turney, C., Umbanhower, C., Vandergoes, M., Vanniere, B., Vescovi, E., Walsh, M., Wang, X., Williams, N., Wilmshurst, J., Zhang , J.H.. 2008. Changes in fire regimes since the Last Glacial Maximum: an assessment based on a global synthesis and analysis of charcoal data. Climate Dynamics, Vol. 30, No. 7-8, pp. 887-907, June 2008. [DOI 10.1007/s00382-007-0334-x].

Tang, M. & Reiter, E.R. 1984. Plateau monsoons of the northern hemisphere: a comparison between North America and Tibet. Monthly Weather Review 112: 617-637.

Whitlock, C. & Bartlein, P.J. 1993. Spatial variations of Holocene climatic change in the Yellowstone region. Quaternary Research 39: 231-238.

Whitlock, C., Bartlein, P.J., Marlon, J. Brunelle, A., Long, C. 2003. Holocene fire reconstructions from the Northwestern U.S.: an examination at multiple

time scales. Second International Wildland Fire Ecology and Fire Management Congress (extended abstract): 4C.1-5. <http://ams.confex.com/ams/pdfpapers/66514.pdf>

Whitlock, C., Bartlein, P.J., Van Norman, K.J. 1995. Stability of Holocene climate regimes in the Yellowstone Region. Quaternary Research 43: 433-436.

Whitlock, C., Marlon, J., Briles, C., Brunelle, A., Long, C., Bartlein, P. 2008. Long-term relations among fire, fuel, and climate in north-western US based on lake-sediment studies. International Journal of Wildland Fire 17: 72-83.

Whitlock, C. & Millspaugh, S.H. 1996. Testing the assumptions of fire-history studies: An examination of modern charcoal accumulation in Yellowstone National Park, USA. Holocene 6: 7-16.